基于二维材料非线性效应的多波长超快激光器研究进展(特邀)

郭 波

(哈尔滨工程大学 纤维集成光学教育部重点实验室,黑龙江 哈尔滨 150001)

摘 要:多波长超快激光器在光通信、医学诊断和光学传感等各种应用中有着十分重要的应用前景。2009 年以来,石墨烯、拓扑绝缘体、过渡金属硫化物和黑磷等二维材料在超快光子学领域的发展非常快速。它们独特的非线性光学特性,使之能够被用作快速响应、宽带运转的可饱和吸收体且能够容易地集成到激光器中。研究发现,基于二维材料的非线性光学器件是研究激光器内非线性脉冲动力学演化的理想平台。在文中,回顾了二维材料在多波长超快激光器中应用的最新进展。进而,阐述了多波长的耗散孤子、矩形脉冲和亮暗孤子对等脉冲类型。最后,提出了这类多波长超快激光器面临的挑战和应用前景。

关键词:二维材料; 锁模激光器; 非线性光学现象; 多波长; 孤子

中图分类号:TN248 **文献标志码**:A **DOI**:10.3788/IRLA201948.0103002

Recent advances in multi-wavelength ultrafast lasers based on nonlinear effects of 2D materials(invited)

Guo Bo

(Key Lab of In-Fiber Integrated Optics of Ministry of Education, Harbin Engineering University, Harbin 150001, China)

Abstract: Multi-wavelength ultrafast lasers play an important role in a variety of applications ranging from optical communications to medical diagnostics and optical sensing. Two-dimensional (2D) materials, including graphene, topological insulators, transition metal dichalcogenides, and phosphorene, have witnessed a very fast development of both fundamental and practical aspects in ultrafast photonics since 2009. Their unique nonlinear optical properties enable them to be used as excellent saturable absorbers with fast responses and broadband operation and can be easily integrated into lasers. Here, we review the recent advances in the exploitation of these 2D materials in multi-wavelength ultrafast lasers. Interestingly, study found that, 2D materials-based nonlinear optical device is an ideal platform for nonlinear pulse dynamics study. Thus, versatile pulse patterns, including dissipative soliton, rectangular pulse, and bright-dark soliton pair, are also demonstrated. Finally, current challenges and future application opportunities of 2D materials-based multi-wavelength ultrafast lasers are presented.

Key words: two-dimensional materials; mode-locked lasers; nonlinear optical phenomenon; multiwavelength; soliton

收稿日期:2018-08-05; **修订日期**:2018-09-03

基金项目:国家自然科学基金(61575051;61875043);“十三五”装备预研共用技术和领域基金(6140414040116CB01012);哈尔滨工程大学 111 项目(B13015)

作者简介:郭波(1980-),男,副教授,硕士生导师,博士,主要从事二维材料光电器件、超快光纤激光技术、光纤光栅及中红外激光器等方面的研究。Email:guobo512@163.com

0 引 言

自 20 世纪 60 年代 Snitzer 提出将光纤技术应用于激光器以来，超快激光器一直是国际上激光领域重要的研究热点[1]。多波长锁模激光器作为超快激光器家族中的一员，因具有输出波长数目多、脉冲宽度短、峰值功率高、工作波段宽等优点而成为光通信、生物医学研究、非线性光学、传感和激光雷达等领域的关键工具，如图 1 所示，逐渐成为众多科学家关注的一个焦点课题[2-3]。

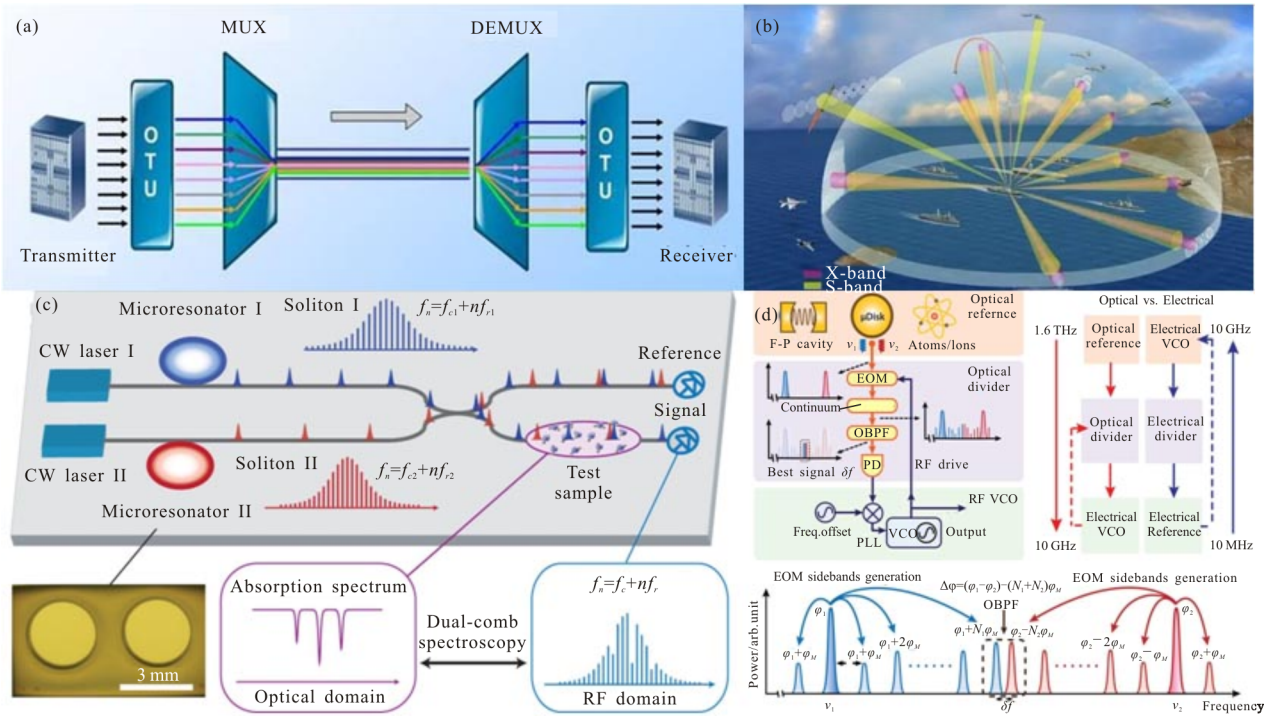

图 1 多波长超快激光器的典型应用：(a) 密集波分复用系统；(b) 相控阵雷达；(c) 双频率梳及其应用[2]；(d) 微波产生[3]

Fig.1 Typical applications of multi-wavelength ultrafast lasers: (a) Dense wavelength division multiplexing system; (b) Phased array radar; (c) Dual-frequency comb and its applications [2]; (d) Microwave generation [3]

为实现多波长锁模激光器，通常需要在腔内插入一个锁模器件和一个滤波器件，从而将连续激光变为一串由多个不同波长组成的激光脉冲[4]。对于前者，已有几种主动[5-14]和被动锁模技术[15-56](如：非线性光纤环形镜[15-21]、非线性偏振旋转[22-42]、半导体饱和吸收镜[43-51]以及碳纳米管[52-56])被用来实现超快脉冲输出。与主动锁模方案相比，被动技术更具优势，例如，结构简单、紧凑，成本低，不需要调制器且容易实现具有高峰值功率的激光脉冲等。对于后者，许多直接方法(如：采样光栅[6]和高双折射光纤[11,13-15])和间接方法(如：在高非线性光纤中产生四波混频效应或受激布里渊散射[26])，被用来实现多波长激光输出。通过这些方法，使腔内功率在不同波长间重新分配，有效抑制增益光纤均匀展宽引起的模式竞争、跳变而实现多波长激光输出。例如，1992 年，英国南安普顿大学 Matsas 等人利用非线性偏振旋转实现了双波长孤子锁模掺铒光纤激光器[22]。2009 年，新加坡南洋理大学唐定远课题组利用半导体饱和吸收镜实现了多波长耗散孤子光纤激光器[43]。2011 年，北京航空航天大学郑铮课题组利用碳纳米管和腔内损耗机制实现了可切换的双波长孤子光纤激光器[52]。不过，这些方法也有不足，如：锁模条件非常严格、需要仔细调整腔内参数、易受光纤运动影响、制备工艺复杂及工作带宽较窄等。同时，研究发现，高非线性在多波长激光脉冲的形成和演化中起着重要作用。为此，多波长超快激光领域的研究人员亟需寻找同时具备饱和吸收和高非线性的新型光子学器件。

2004 年，英国曼彻斯特大学 Geim 和 Novoselov 利用透明胶带成功制备出了石墨烯[57]，如图 2 所示。它是单层碳原子以六方晶格规律排布形成的二维晶体结构，碳原子之间以共价键链接而呈现出蜂窝状的网状结构。此后，更多类型的二维材料，包括：拓扑

绝缘体、六方氮化硼、过渡金属硫化物、黑磷、金属烯和石墨化氮化碳以及金属有机框架化合物，如图 2 所示，也引起了物理学、化学和材料领域研究人员的极大兴趣和关注[58-60]。研究发现，二维材料具有“对顶圆锥”型的能带结构，从而表现出十分新奇的光电特性，包括：工作波段宽、调制深度可调、恢复时间快、饱和吸收阈值低、非线性折射率高、热损伤阈值高等优点，使之成为理想的激光脉冲整形器件，探索这类二维材料在激光器件中的应用成为目前光电子领域的热点问题之一[61-68]。例如，2009 年，新加坡南洋理工大学鲍桥梁等人[61]和英国剑桥大学孙志培等人[62]发现了石墨烯饱和吸收特性并在实验中实现了孤子脉冲输出。不过，目前，人们多侧重于利用这类二维材料的饱和吸收特性在单波长锁模方面的研究，而较少探索这类材料同时具有的高非线性。研究发现，腔内具有高非线性介质的激光器，有利于产生多波长激光。可以设想，基于二维材料的非线性光学器件在激光器内，可以充当双重功能，即饱和吸收和高非线性，非常有利于多波长锁模脉冲产生。同时，二维材料非线性光学器件也是探索激光脉冲传输及其非线性动力学演化的理想工具。

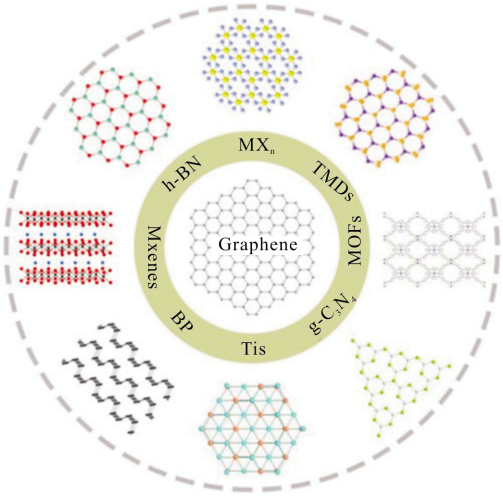

图 2 不同类型二维材料的示意图，例如：石墨烯、六方氮化硼(h-BN)、过渡族金属硫化物(TMDs)、金属有机框架化合物(MOFs)、金属化合物(MX_n)、金属烯(MXenes)、拓扑绝缘体(TIs)以及黑磷(BP)

Fig.2 Schematic illustration of different kinds of 2D materials, such as graphene, h-BN, TMDs, MOFs, MX_n, MXenes, TIs, and BP

在文中，将简要回顾基于二维材料的多波长超快激光器的研究进展，并对相关的非线性光学现象，包括耗散孤子、矩形脉冲和亮暗孤子对，进行深入分析。

2 二维材料的制备、非线性光学性质及器件制作

2.1 材料制备

二维层状材料的制备方法主要有两种：自上向下的方法，通过打破层间的范德瓦尔斯力，将散状材料剥离到单层或几层二维纳米片，以及直接从分子水平合成二维材料的自下而上的方法。下面简要介绍机械剥离法、液相剥离法、气相沉积法以及脉冲激光沉积法等。

2.1.1 机械剥离法

二维材料层之间是通过微弱的范德瓦尔斯力结合的，施加外力，可以将块状二维材料剥离而得到单层或少层的二维材料[57]。目前，通过这种方法成功地将块状的二维材料剥离至几层甚至单层厚度。该方法主要采用胶带黏住块状材料的两侧面，通过反复剥离，得到二维材料。采用该方法可以得到尺寸在几微米到几十微米之间的二维材料，最大尺寸甚至可达到毫米量级。机械剥离法操作简单且制备出的二维材料的晶体结构较为完整，非常适合用来制造纳米光电子器件。但是，这种方法制备出的二维材料通常呈散片状，产量极低，重复性较差且尺寸和层数不易控制，因此，不适合大规模制备。

2.1.2 液相剥离法

液相剥离法是制备二维层状材料的有效方法[59-60]，该方法的原理是：将粉末或块状二维材料放在含有表面匹配能的溶剂里，然后，在超声作用下进行分散和剥离，接着，使用离心机进行分离，去除层数较多的二维材料，就获得了少层，甚至单层二维材料。该方法一般在液体中进行，还要用超声辅助，在这个过程中，超声频率及溶剂的选择对二维材料剥离的结果有重要影响。选择溶剂时，主要参考其具有的表面张力。一般选取有机溶剂异丙醇、二甲基亚砜、丁内酯等作为超声分散的液体。由于液相超声分散剥离法操作十分简单便捷，且可以批量化生产，因而具有实现工业化生产的巨大潜力，但其剥离程度和效率有待提高。

2.1.3 气相沉积法

气相沉积法也是制备二维材料的主要方法之

一[65-67]，其优点是可以生长出质量高、面积大、层数可控的二维材料且基体铜箔等金属的价格便宜，适合工业化大规模生长，目前已被广泛应用于制备二维材料。该方法的优势在于可控、可获得大面积薄膜，因此，气相沉积法得到广泛采用，具有非常大的发展潜力。

2.1.4 脉冲激光沉积(Pulsed Laser Deposition，PLD)法

PLD 是一种利用脉冲激光对物体进行轰击，然后将轰击出来的物质沉淀在不同的衬底上，得到沉淀或者薄膜的一种技术[68]。其原理一般可以分为以下四个阶段：激光辐射与靶的相互作用、熔化物质的动态、熔化物质在基片上的沉积、薄膜在基片表面的成核与生成。

PLD 技术具备许多特殊的优势：具有良好的保成分性；沉积速率高，试验周期短，衬底温度要求低，制备的薄膜均匀；脉冲激光沉积能够制备高质量的纳米量级薄膜。等离子体粒子束流携带很高的动能，具有显著增强二维生长抑制三维生长的作用，可以促进薄膜沿平面生长，因而能避免分离成核岛状，获得连续均一的薄膜；工艺参数任意调节，对靶材种类没有限制；便于清洁处理，可以制备多种薄膜材料。

2.2 二维材料的非线性光学性质

近年来，二维材料由于具有可调控光电特性、超宽工作波长带宽、高电子迁移率、高热导系数及光纤可兼容性等优点，引起了物理、化学、材料等领域研究人员的广泛兴趣，如表 1 和图 3 所示，探索这类材料的非线性光学性质，是当前光学研究的热点之一。

表 1 二维材料的非线性光学性能总结

Tab.1 Summary of the nonlinear optical parameters of 2D materials

Mater.	Laser parameters	NLO response	α_0/cm^{-1}	α_{NL}/cm·GW^{-1}	Im$\chi^{(3)}$/esu	Ref.
G	800 nm, 1 kHz, 100 fs	SA	17.85	$-(1.52\pm0.4)\times10^{-2}$	$-(8.7\pm2.4)\times10^{-15}$	[69]
GO	532 nm, 1 Hz, 25 ns	SA	426.55	1.44	-	[70]
rGO	532 nm, 1 Hz, 25 ns	SA	880.67	2.67	-	[68]
Bi_2Se_3	1 562 nm, 20.8 MHz, 1.5 ps	SA	-	-	0.86(n_2)	[80]
Bi_2Te_3	1 550 nm, 35 fs	—	-	-	0.2×10^{-17}(n_2)	[79]
MoS_2	800 nm, 1 kHz, 100 fs	SA	11.22	$-(2.42\pm0.8)\times10^{-2}$	$-(1.38\pm0.45)\times10^{-14}$	[82]
WS_2	800 nm, 1 kHz, 40 fs	SA	7.22×10^5	-397 ± 40	$-(1.78\pm0.16)\times10^{-9}$	[83]
$MoSe_2$	800 nm, 1 kHz, 100 fs	SA	7.93	$-(2.54\pm0.6)\times10^{-2}$	$-(1.45\pm0.34)\times10^{-15}$	[68]
WSe_2	1 064 nm, 20 Hz, 25 ps	2PA	-	1.9 ± 0.57	$-(6.35\pm1.35)\times10^{-12}$	[68]
BP	800 nm, 10 kHz	SA	8.7	-1.38×10^{-2}	-7.85×10^{-15}	[87]
Si	1 540 nm, 220 fs	—	-	-	0.45×10^{-17}(n_2)	[80]

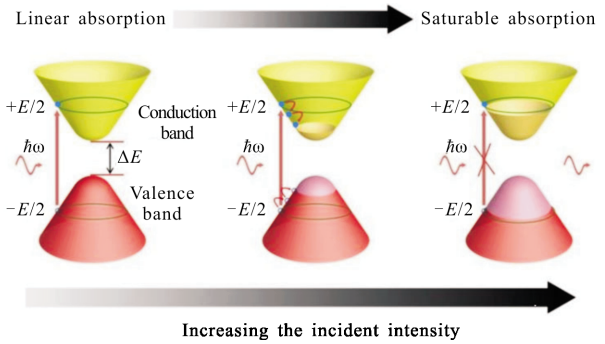

图 3 二维材料的饱和吸收机制：在光激发下，电子的带间跃迁(左)；热载流子的转移及平衡(中)；光吸收的阻塞(右)

Fig.3 Saturable absorption mechanism of 2D materials: (Left) Interband transition of the electron due to light excitation; (Middle) Hot carriers lend to thermal balance; (Right) Blocking of absorption for light

石墨烯是一种由碳原子以 sp^2 杂化方式连接的无带隙的狄拉克材料[57]。研究发现，它具有超快时间响应(~100 fs)、宽带光吸收、可控调制深度、低饱和吸收光强度等优异性能而可以作为饱和吸收体，被广泛用于锁模或调 Q 脉冲的产生。此外，石墨烯还是一种优良的光学克尔介质，其三阶非线性极化率为 10^{-7}，这是碳纳米管的 10 倍，高出硅材料近 7 个数量级。

2009 年，南开大学陈永胜和田建国课题组研究了氧化石墨烯在 532 nm 处的纳秒和皮秒非线性光学性质[69]，如图 4(a)~(c)所示。结果表明，在皮秒脉冲情况下，双光子吸收占主导地位，而激发态非线性在纳秒脉冲的情况下起着重要作用。2010 年，英国埃克塞特大学 Hendry 课题组利用四波混频研究了单

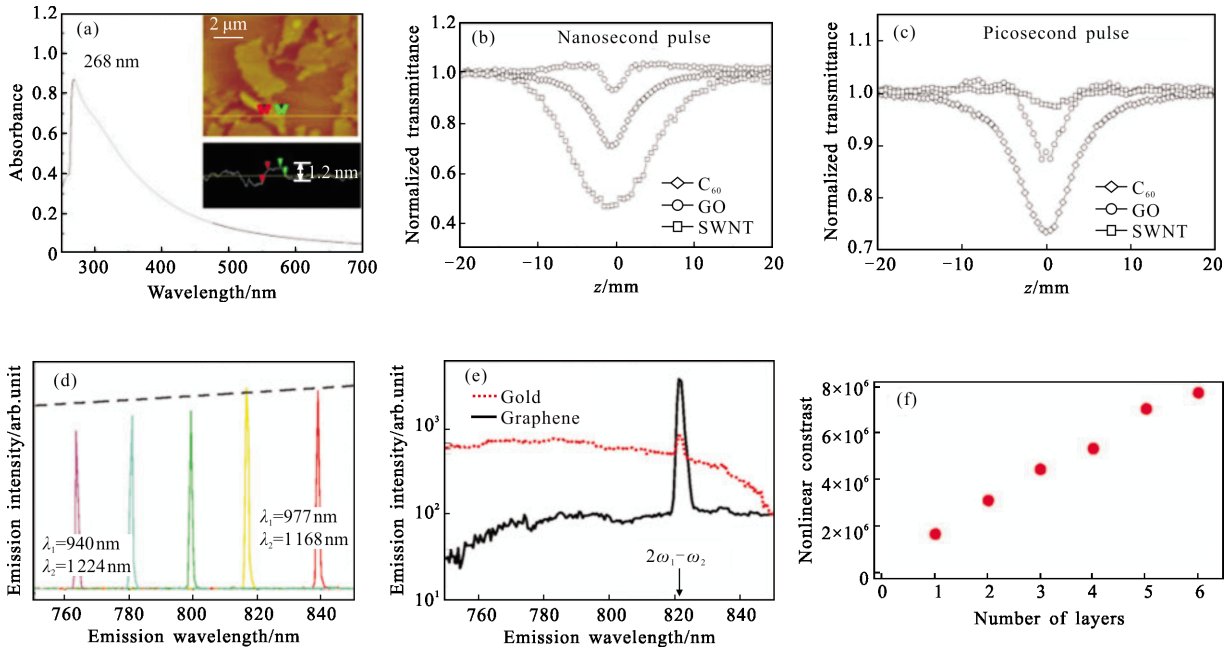

图 4 石墨烯和氧化石墨烯的非线性光学性质:(a)氧化石墨烯在 N,N-二甲基甲酰胺(DMF)中的紫外吸收谱,插图是氧化石墨烯的原子力显微镜照片;(b)、(c)分别为氧化石墨烯(GO)、单壁碳纳米管(SWCNT)及富勒烯(C_{60})在 DMF 和甲苯中,泵浦为纳秒和皮秒脉冲时的开孔 Z 扫描曲线[69];(d) 用不同波长泵浦脉冲激发石墨烯片时的发射光谱,虚线表示波长的依赖性;(e)与 4 nm 厚的金膜相比,泵浦波长(969 nm,1179 nm)激发的单层石墨烯的发射光谱;(f)在四波混频过程中,非线性对比度与石墨烯层数目之间的关系[70]

Fig.4 NLO properties of graphene and graphene oxide (a) UV absorption of GO in N, N-Dimethyl formamide (DMF). The inset is an AFM image of GO sheets; (b),(c) Open aperture Z-scan curves of GO, Single-walled carbon nanotubes (SWCNTs) in DMF, and C_{60} in toluene for nanosecond and picosecond pulses, respectively. Reproduced with permission[69]. Copyright 2009, American Institute of Physics; (d) Emission spectra of a graphene flake excited with pump pulses of different wavelengths, (λ_1, λ_2). The dashed line represents the wavelength dependence; (e) Emission spectra of a graphene monolayer excited with pump wavelengths (969 nm, 1179 nm), compared to the emission of a 4 nm thick gold film; (f) The contrast in four-wave mixing images as a function of the number of graphene layers. Reproduced with permission[70]. Copyright 2010, American Physical Society

层和少层石墨烯薄膜的非线性光学性质响应[70],如图 4(d)~(f)所示。他们指出,石墨烯在近红外光谱区域表现出非常强的三阶非线性光学响应,这可能起源于带间电子跃迁,比没有这种跃迁的介电材料所观察到的非线性大 8 个数量级。

拓扑绝缘体(Topological Insulators,TIs)是一类非常特殊的绝缘体,这类材料体内的能带结构是典型的绝缘体型,在费米能级处存在能隙;而在该类材料表面则总是存在着可以穿越能隙的狄拉克型金属边缘或表面态[71-77]。2004 年至今,人们发现了几十种不同的拓扑绝缘体:第一代以 HgTe 量子阱为代表;第二代以 $Bi_{1-x}Sb_x$ 合金为代表,由 Hsieh 等人于 2008 年首次在实验上制备成功;第三代以 Bi_2Se_3,Bi_2Te_3[72],Sb_2Te_3 等化合物为代表。

2012 年 8 月,新加坡南洋理工大学 Bernard 等人首次研究了拓扑绝缘体 Bi_2Te_3 在 1550 nm 波长处的饱和吸收特性[78]。此后,湖南大学的张晗和文双春课题组采用 Z 扫描技术研究了拓扑绝缘体 Bi_2Te_3[79] 和 Bi_2Se_3[80]的宽带三阶非线性:当激发波长为微波时,表现出饱和吸收行为;当激发波长为 800 nm 时,其饱和强度和调制深度分别为 10.12 GW/cm² 和 61.2%;折射率高达 10^{14} m²/W,约为块状介质的一百万倍,其实验装置和结果分别如图 5 (a)~(f)所示。之后,一系列的实验证实,包括 Bi_2Se_3、Bi_2Te_3、

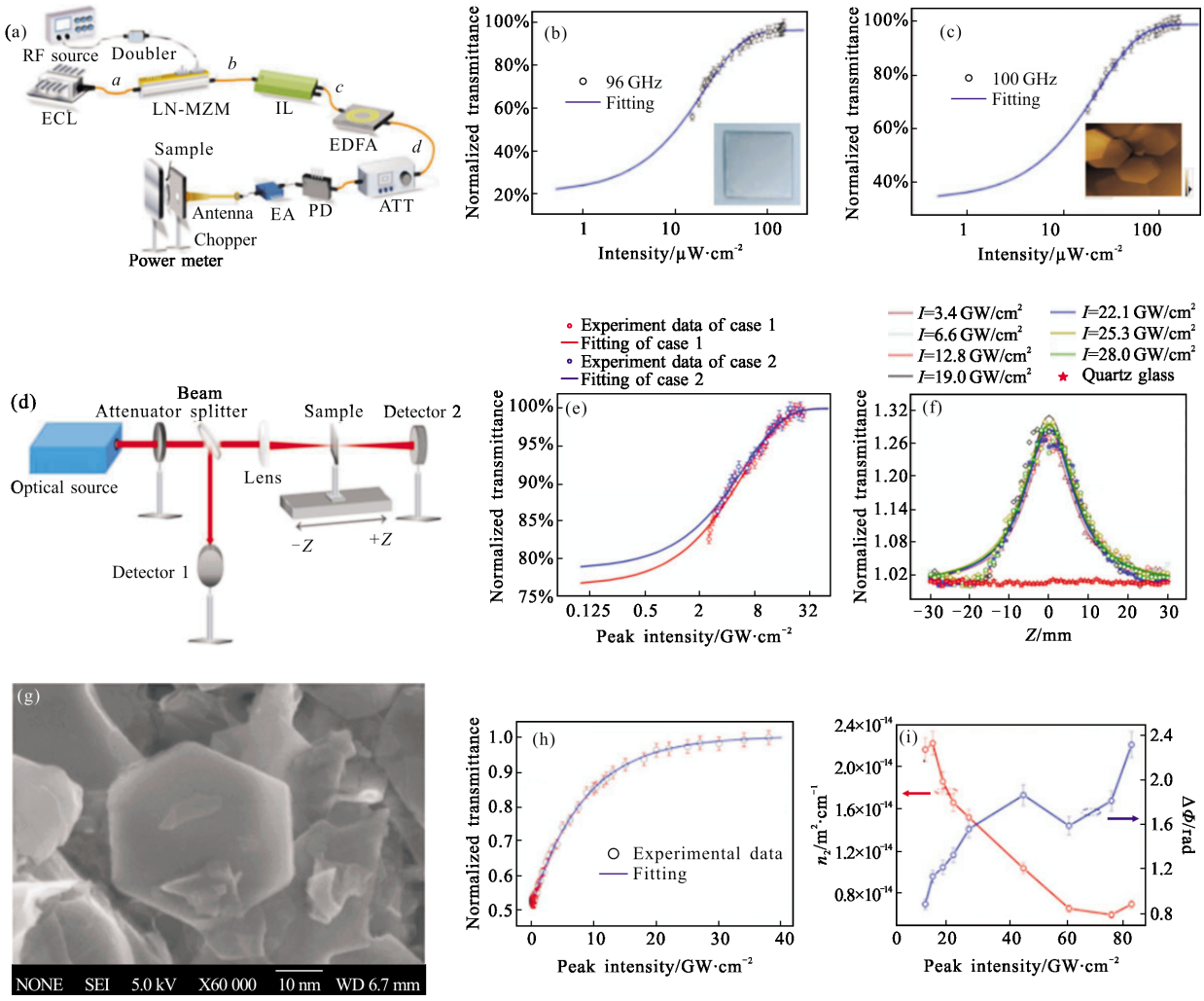

图 5 拓扑绝缘体的非线性光学性质：(a)微波时，饱和吸收的测量示意图；(b)、(c)不同微波频率下，Bi_2Te_3 饱和吸收特性；(d)Z 扫描实验装置示意图；(e)归一化透射率与输入峰值强度之间的关系；(f)在 800 nm 处的开孔 Z 扫描曲线[79]；(g)Bi_2Se_3 的 SEM 照片；(h)归一化透射率与输入峰值强度之间的关系；(i)峰值强度、相位差与折射率之间的关系[80]

Fig.5 NLO properties of topological insulator. (a) Schematic of the microwave generation and saturable absorption measurement; (b), (c) saturable absorption of Bi_2Te_3 at different microwave frequencies; (d) Schematic of the Z-scan experimental setup; (e) Relation between normalized transmittance and input peak intensity; (f) Open Z-scan curve at 800 nm. Reproduced with permission[79]. Copyright 2014, Optical Society of America; (g) SEM images of Bi_2Se_3; (h) Relation between normalized transmittance and input peak intensity; (i) Dependence of $\Delta\Phi$ and n_2 on peak intensity. Reproduced with permission[80]. Copyright 2013, Optical Society of America

Sb_2Te_3 及 Bi_2SeTe_2 在内的拓扑绝缘体可被视为一种饱和吸收体用来实现 0.5~3 μm 波段的锁模或调 Q 激光器[68]。

过渡族金属硫化物(transition-metal dichalcogenides，TMDs)，可以表达为 MX_2(M=Mo，W，Nb，Re，等；X=S，Se，Te，等)，由于在电子和光电子方面具有优异的特性(饱和吸收、高非线性、限幅性等)，也引起了物理、化学和材料领域研究人员的极大关注[81]。研究发现，TMDs 具有宽带可调谐的带隙、较高的载流子迁移率，并表现出优良的三阶非线性光学性质，包括宽带饱和吸收、双光子吸收及高非线性等。例如，中国科学院上海光学精密机械研究所王俊课题组[82]以及香港理工大学雷党愿[83]课题组采用开孔 Z 扫描技术分别揭示了 MoS_2 的超快非线性光学性质，如图6 所示。利用 MX_2 的饱和吸收特性，研究人员先后实现了锁模或调 Q 激光器等[68]。

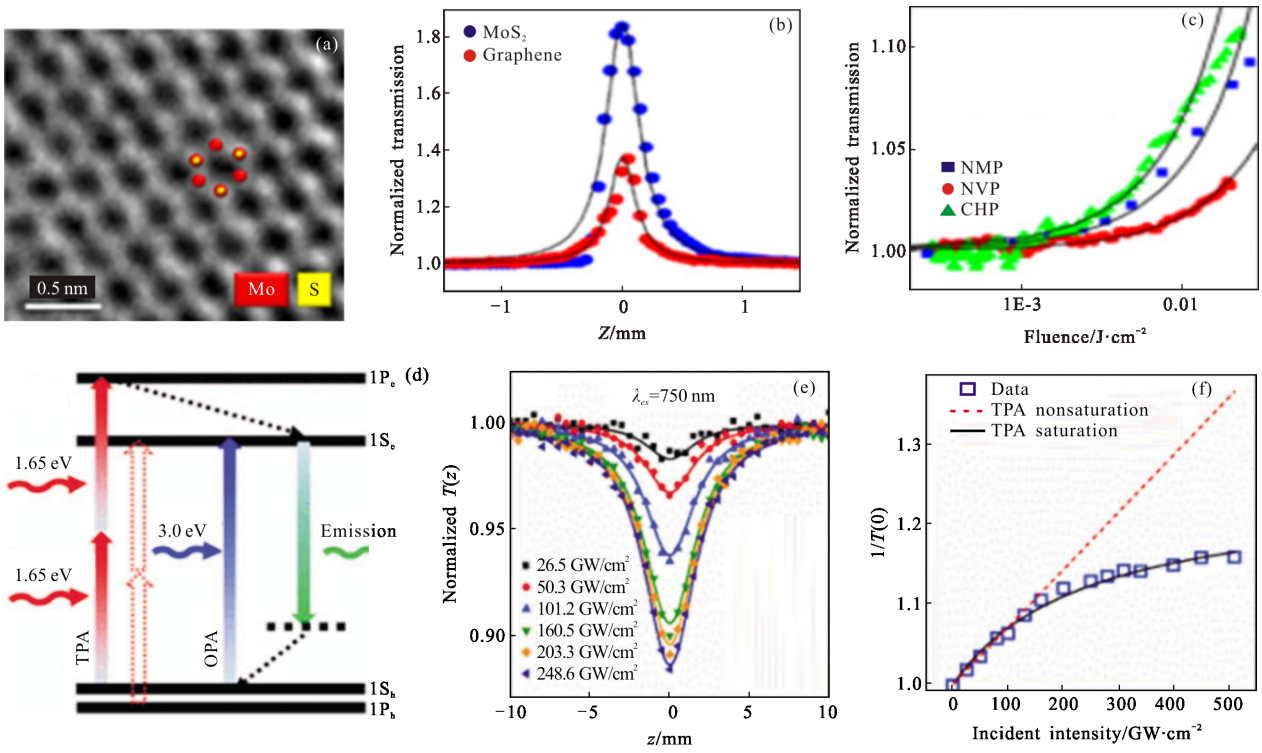

图 6 二硫化钼的非线性光学性质:(a) MoS_2 纳米片的高分辨率电子显微镜照片;(b)在 800 nm、100 fs 脉冲激光激励下,MoS_2(t=34.4%)和石墨烯(t=16.5%)溶液的开孔 Z 扫描结果;(c)三种分散体的能量密度与归一化透射率之间的关系[82];(d) MoS_2 纳米点中,单光子和双光子跃迁的能级示意图;(e)在 750 nm,MoS_2 量子点在不同入射强度下的 Z 扫描测试结果;(f)在焦点处,透射功率与从(e)中提取的入射强度(空心方块)之间的关系[83]

Fig.6 NLO properties of MoS_2 dispersions. (a) High-resolution TEM image for MoS_2 nanosheet; (b) open-aperture Z-scan results under the excitation of 100 fs pulses at 800 nm for the MoS_2 (t=34.4%) and graphene (t=16.5%) dispersions; (c) Normalized transmission as a function of fluence for the three dispersions. Reproduced with permission[82]. Copyright 2013, American Chemical Society. (d) Schematic illustration of the discrete energy levels for one- and two-photon allowed transitions in MoS_2 NDs; (e) Incident-intensity dependent Z-scan responses of the MoS_2 NDs at wavelength 750 nm; (f) Reciprocal power transmission at the focal point vs incident intensity (hollow squares) extracted from, (e) Reproduced with permission[83]. Copyright 2016, American Chemical Society.

黑磷是热力学上最稳定的磷的同素异形体,其直接带隙由层数决定,可在 0.3 eV(块体)和 2 eV(单层)之间变化[84]。宽带可调谐的带隙、较高的载流子迁移率、在中红外范围内强的光物质相互作用以及独特的各向异性,使得黑色磷成为一种良好的非线性光学材料,特别是近红外和中红外光电子器件具有巨大的潜力[85]。此外,黑磷还表现出丰富的三阶非线性光学性质,包括宽带饱和吸收性、高非线性等[86]。例如,张晗课题组通过 Z 扫描技术,实验验证了多层黑磷的宽带可饱和吸收行为[87],如图 7 所示。利用这些光学性质,研究人员先后实现了锁模和调 Q 光纤及固体激光器等[68]。

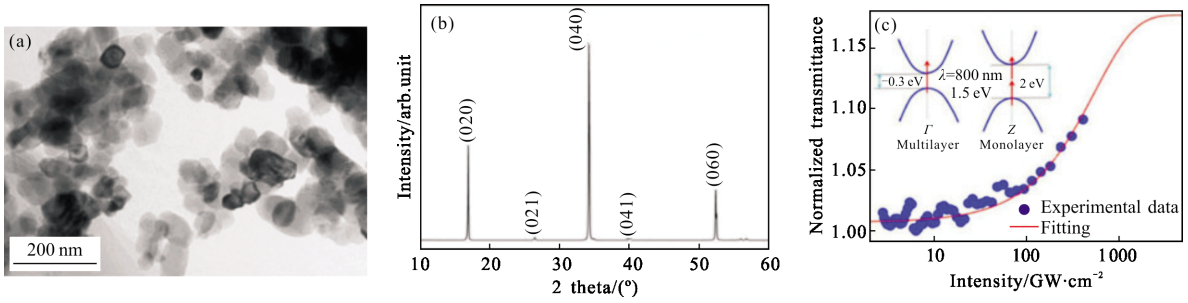

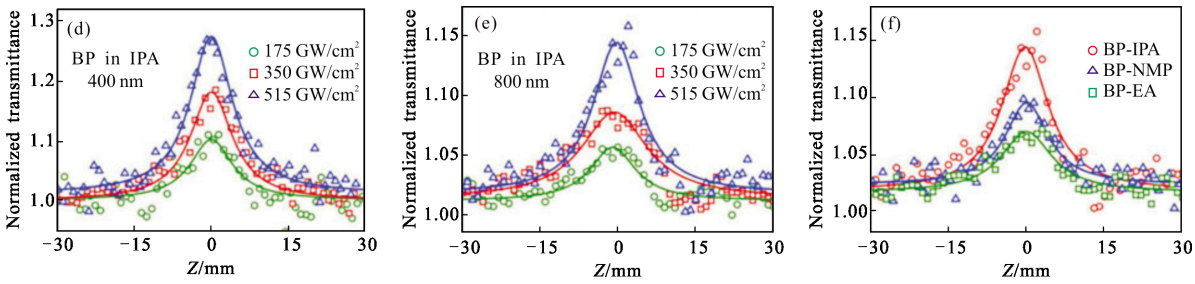

图 7 多层黑磷的宽带非线性光学响应[87]：一种新兴的近红外和中红外光学材料；(a) 所制备黑磷的电子显微镜照片；(b) 黑磷粉末的 X 射线衍射图样；(c) 黑磷归一化透射率和输入强度之间的关系；(d)，(e)不同强度时黑磷的开孔 Z 扫描测试结果；(f)当强度为 515 GW/cm² 时，黑磷在 IPA，NMP 及 EA 中的开孔 Z 扫描测量结果

Fig.7 Broadband nonlinear optical response in multilayer black phosphorus[87]: an emerging near-, and mid-infrared optical material. (a) TEM image of as-prepared BP; (b) XRD pattern of BP powder; (c) Relation between normalized transmittance and input intensity for BP; (d), (e) are the open aperture Z-scan measurements of BP under different intensities, respectively; (f) The open aperture Z-scan measurements of BP in IPA, NMP and EA at intensities of 515 GW/cm². Reproduced with permission. Copyright 2015, Optical Society of America.

2.3 器件制作

为了将二维材料转移到激光器腔内，日本东京大学的 Martinez 和芬兰阿尔托大学的孙志培总结了石墨烯的转移方法[88]，如图 8 所示。这些方法同样适用于其他二维材料。

首先，二维材料可经机械剥离、光沉积或制成聚合物薄膜转移到两连接器之间构成三明治结构[65]，如图 8(a)所示；

其次，注入光纤微流通道或光子晶体光纤中，如图 8(b)和 8(c)所示，该方法制备的饱和吸收体具有非常强的光与物质相互作用，同时，表现出相对大的插入损耗及在光子晶体光纤孔隙部分容易产生失真模式[66-67]；

第三，为了利用倏逝场的相互作用机制，将二维材料沉积在 D 型光纤或拉锥光纤上，如图 8(d)和 8(e)所示，该方法制备的非线性光学器件可以承受非常高的功率及很长的相互作用长度，但不宜获得均匀分布的二维层状材料薄膜[68]。

第四，直接将二维材料集成到微纳激光器中[88]，如图 8(f)所示。

此外，将二维材料沉积在玻璃或陶瓷上制成“自由空间”型的吸收镜也是一种有效的转移方法[68]。

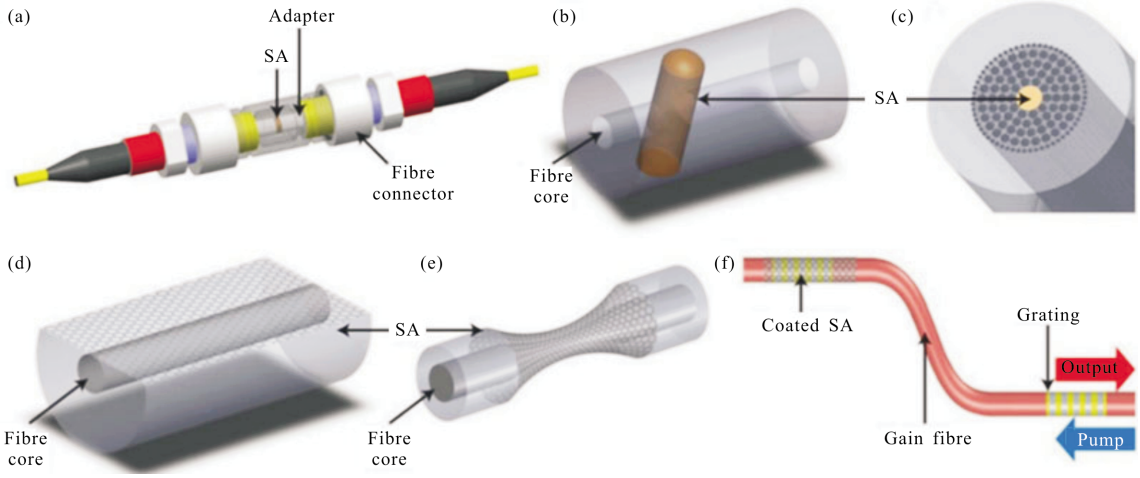

图 8 各种光纤型饱和吸收体的制备方法[88]

Fig.8 Various SA integration methods for fibre devices[88]

3 多波长超快激光的运转机制

调制器件：主要是指主动锁模器件中的振幅或相位调制器，该方式需要保证每个波长经过调制器时保持相位同步；

直接滤波器件：包括取样光栅、高双折射光纤、马赫-曾德尔干涉仪及萨格纳克干涉环等。

非线性偏振旋转(Nonlinear polarization rotation，NPR)或非线性光纤环形镜(Nonlinear optical loop mirror，NOLM)：主要是指在谐振腔内引入强度相关损耗，来实现稳定的多波长光纤激光器。当脉冲在NPR锁模光纤激光器中传输时，由于脉冲功率的峰值限制效应限定了单个波长的功率水平，从而大大减弱了相邻波长间的强烈模式竞争，实现了常温下稳定的多波长脉冲激光运转。此外，研究发现，NOLM的透射率与入射光强度有关，脉冲经过NOLM后，功率较强的脉冲会有较大的损耗，功率较弱的脉冲会有较小的损耗，从而有效地抑制光纤激光器中的波长竞争，实现多波长脉冲激光输出。不过，为了实现较强的非线性强度相关损耗，在NOLM或NPR谐振腔中需要接入长度为几千米至十几千米的单模光纤，激光器的谐振腔长度比较长。

非线性效应：是指在高非线性光纤或者特种光纤中产生四波混频效应或受激布里渊散射，通过这些非线性效应，功率在不同波长间重新分配，这就有效抑制增益光纤均匀展宽引起的模式竞争、跳变，从而实现了多波长脉冲输出。

与其他方法相比，基于非线性效应的多波长锁模光纤激光器具有全光纤化、成本低等优势。由于二维材料特殊的“对顶圆锥”型能带结构，可以实现宽波长范围内饱和吸收和高非线性，因此，二维材料光学器件在激光器腔内可以等效为一个双功能器件，既可以利用其优良的饱和吸收特性用来锁模，又可以利用其显著的高非线性效应用来产生多波长激光，因此，基于二维材料高非线性效应的多波长光纤激光器具有较强的应用潜力。

4 多波长超快激光器研究进展

2010年，厦门大学电子工程系罗正钱课题组利用石墨烯沉积的光纤器件实现了双波长调Q掺铒光纤激光器[89]，如图9(a)~(c)所示。此后，研究人员发展

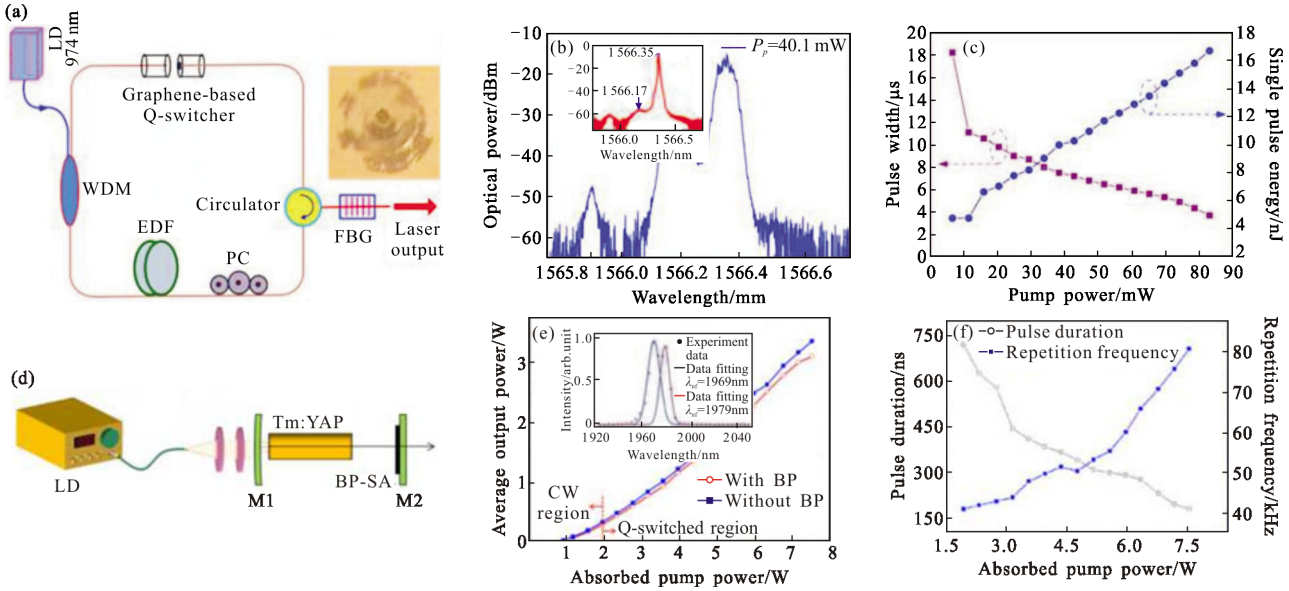

图9 基于石墨烯和黑磷饱和吸收体的双波长调Q运转：(a)光纤激光器的实验装置示意图，插图：沉积石墨烯后的光纤跳线端面照片；(b)双波长调Q激光光谱，插图：腔内没有石墨烯时的连续波输出光谱；(c)脉冲持续时间和脉冲能量与入射泵功率之间的关系[89]；(d)基于黑磷饱和吸收体的固体激光器实验装置示意图；(e)平均输出功率与吸收泵浦功率、发射光谱的关系；(f)脉冲宽度、重复频率与所吸收泵浦功率的关系[96]

Fig.9 Dual-wavelength Q-switching operation based on the graphene SA[89] and BP SAM[96]: (a) Experimental setup of fiber laser, Inset: image of the fiber end face after the graphene was deposited; (b) dual-wavelength Q-switched lasing spectrum, Inset: CW output spectrum without the graphene in the cavity; (c) pulse duration and pulse energy as a function of the incident pump power. Reproduced with permission. Copyright 2010, Optical society of America; (d) the solid laser setup based on BP-SA; (e) average output power versus absorbed pump power and emission spectrum; (f) pulse width and repetition rate versus the absorbed pump power. Reproduced with permission. Copyright 2016, Optical society of America

了大量的多波长调 Q 激光器(光纤[90-93]和固体[94-104]),如表 2 所示。其中,在光纤激光器中,获得了最小脉冲宽度 1.67 μs[92]和最大脉冲能量 229.74 nJ[93]的多波长脉冲激光输出;在固体激光器中,获得了最小脉冲宽度 96 ns[97]和最大脉冲能量 39.5 μJ[96]的多波长脉冲激光输出。

表 2 基于二维材料的多波长调 Q 激光器总结

Tab.2 Summary of the multi-wavelength Q-switched lasers based on 2D materials

2D Materials	Incorporation method	Central wavelength/nm Wavelength number	Repeat rate/kHz	Pulse width/μs	Pulse energy/nJ	Output power/mW	Ref.
Graphene	Sandwiched	1 566.17/1 566.35	3.3-65.9	3.7	16.7	1.1	[89]
Graphene	Sandwiched	1 555.5-1 560, 23 1 027.5-1 037.5, 4	2.8-63 39.8-56.2	25-51 3-3.9	72.5 10.3	4.57 0.58	[90]
Graphene	Sandwiched	1 531.12/1 556.79	12.6-22.8	8.2-26.5	70.2	1.6	[91]
Graphene	Sandwiched	1 550-1 551,11	152.4-267.2	1.67-12.17	-	-	[92]
Graphene	SAM	1 076/1 079.7, solid	45-159	0.096-0.68	11 300	1 080	[97]
Graphene	SAM	1 442.8/1 415, solid	40-101	0.47-1.1	5.95	601	[100]
Graphene	SAM	1 082/1 092, solid	70-133	0.176-2.1	2750	365	[101]
GO	Sandwiched	1 547-1 552, 5	15.36-72.25	2.72-6.8	229.74	16.6	[93]
GO	Injected into PCF	1 553.42/1 553.83	24	-	8.98	0.167	[94]
GO	Sandwiched	1 551.845/1 551.873	24-31	7-13.2	1.7-2.6	0.086	[97]
GO	SAM	1 057.28/1 060.65 (solid)	132-338	0.115-0.31	1340	521	[122]
Bi_2Se_3	SAM	1 077/1 081 (solid)	44.3-94.7	0.72-1.81	834.2	79	[98]
Bi_2Se_3	SAM	1 066.6/1 066.8 (solid)	1-135	0.25-0.55	560	74.2	[98]
Bi_2Se_3	SAM	1 037.14/1 037.69	15.37-59.24	8.46-20.88	0.65	0.038	[102]
MoS_2	SAM	1 025.2/1 028.1 (solid)	94-333	0.182-0.82	1 800	0.6	[99]
WS_2	SAM	1 057/1 061 (solid)	45-70.7	0.591-1	5.19	367	[95]
BP	SAM	1 969/1 979 (solid)	41-81	0.181-0.72	39 500	3 100	[96]

4.1 多波长超快激光器

近年来,研究人员发展了许多基于二维材料器件的多波长超快光纤和固体激光器,如表 3 所示。由于石墨烯具有“对顶圆锥”型的能带结构[62],即导带和价带之间没有带隙,使它对所有波段的光都有吸收作用,从而表现出饱和吸收范围宽、光学非线性强、损伤阈值高及恢复时间快等优势,使之非常适合于多波长激光器方面的探索。

2012 年,厦门大学电子工程系罗正钱课题组利用石墨烯引起的非线性四波混频及其与光纤锥之间形成的倏逝场相互作用,成功研制了一个石墨烯沉积的拉锥器件,并用于掺铒光纤激光器,实现了皮秒量级的四波长锁模光纤激光器[105],如图 10(a)~(c)所示。他们发现,该石墨烯器件不仅可以作为锁模器,而且还能够诱导偏振效应,与腔内的偏振器结合起来,可以构成多波长激光产生的双折射滤波器。此

表 3 基于二维材料的多波长锁模激光器总结

Tab.3 Summary of the multi-wavelength mode-locked lasers based on 2D materials

2D materials	Incorporation method	Central wavelength/nm	Repeat rate/MHz	Pulse width/ps	Pulse energy/nJ	Output power/mW	Ref.
Graphene	Deposited on microfiber	1 529-1 535,4	8.034	8.8	0.42	3.36	105
Graphene	Sandwiched	1 533.4/1 556.11	8.4/9.1	0.9/0.94	1.38	11.36	106
GO	Sandwiched	1 572.93/1 588.37	23.4	12 200	0.65	15.2	107
G-SnO_2-PANI	Sandwiched	1 532/1 557.6	2.13	1.25	1.51	3.2	108
Bi_2Se_3	Sandwiched	1 566-1 570,4	8.83	22	1.1	9.7	109
Bi_2Se_3	Sandwiched	1 527-1 532,3	8.95	-	-	-	110
Bi_2Se_3	Sandwiched	1 547.5-1 552.5,3	8.95	30	1.12	10	111
WS_2	Deposited on microfiber	1 558.54/1 565.99	8.83	0.585	1.14	10.1	112
WS_2	Deposited on microfiber	1 568.55/1 569	2.14	11	6.63	14.2	113
BP	Sandwiched	1 557.2/1 557.7/1 558.2	1.65	9.41	-	-	114
BP	Sandwiched	1 533/1 558	20.82	0.7	1.5	0.07	115
Bi_2Se_3	Deposited on microfiber	1 557.4/1 559.4, harmonic	239/388	1.3	-	-	116
GO	SAM	1 057.28/1 060.23	100	441	-	189	118
Graphene	Deposited on microfiber	1 031.43/1 034.94/1 038.43,DS	0.5515	74.6	6.4	3.52	119
GO	Sandwiched	1 056.5/1 062.3/1 069.5, DS	14.2	-	-	-	120
Bi_2Se_3	Sandwiched	1 561.6/1 562.1, rectangular	3.54	-	-	10	121
GO	Deposited on microfiber	1 061.8/1 068.8, rectangular	1.78	4 230	1.713	3.05	122
rGO	Deposited on microfiber	1 564.6/1 567.4, rectangular	7.9	75 000	-	8	123
Bi_2Se_3	Sandwiched	1 565/1 566, Bright-dark soliton pair	1.09	-	-	-	125

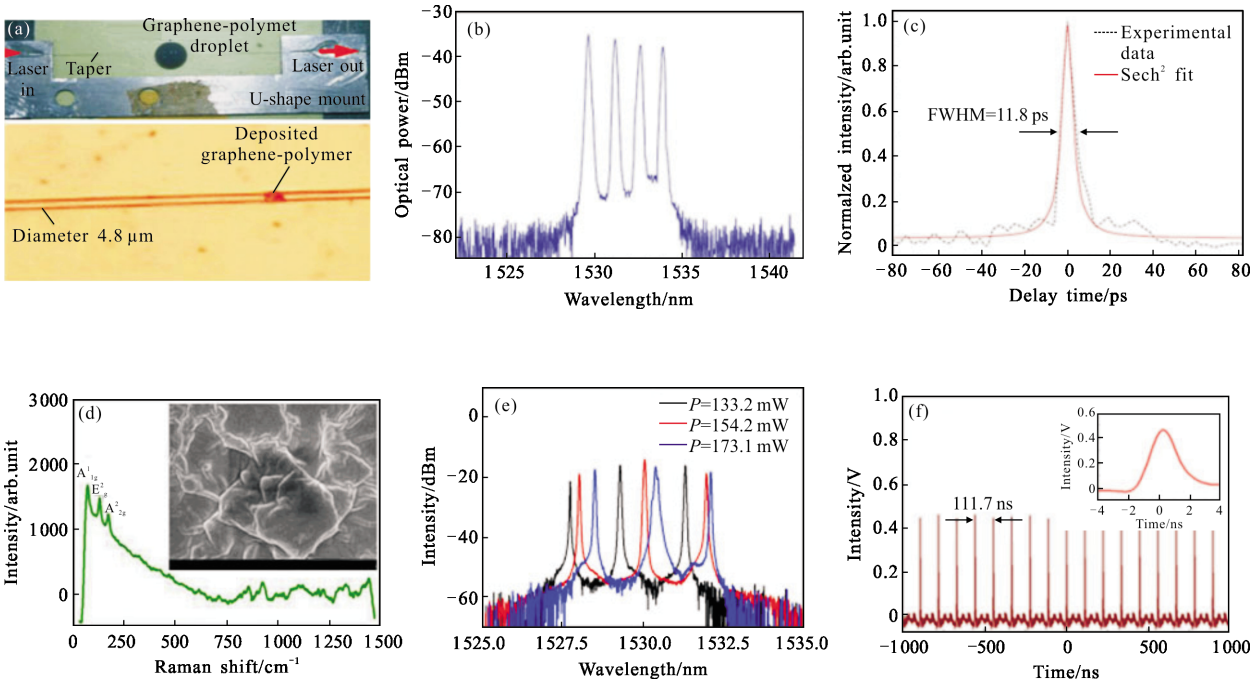

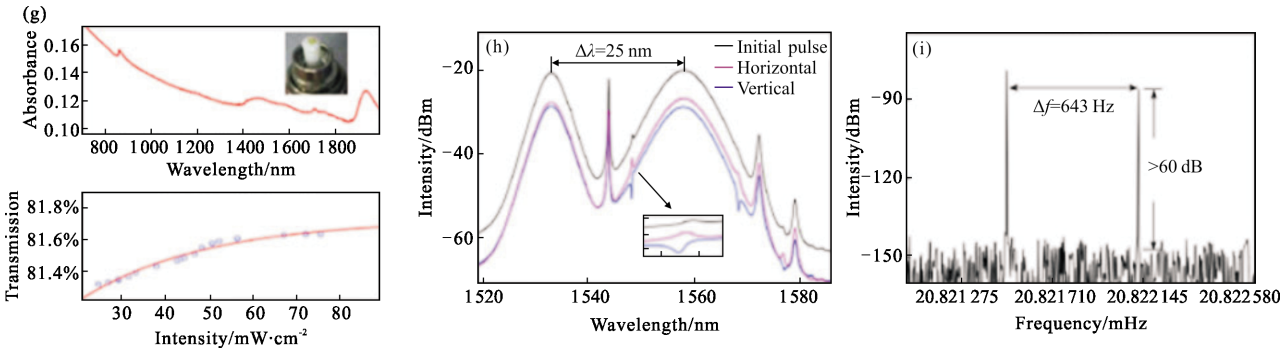

图 10 基于石墨烯、拓扑绝缘体和黑磷饱和吸收体的多波长锁模运转：(a)利用倏逝光在锥形光纤中沉积石墨烯的实验装置示意图；(b)石墨烯拉锥器件的扫描电子显微镜照片；(c)光谱和(d)自相关轨迹[105]；(d)Bi_2Se_3 的拉曼谱(插图：SEM 照片)；(e)光谱和(f)脉冲序列(插图：单脉冲)[111]；(g)黑磷的线性吸收光谱和非线性透射[115]；双波长孤子脉冲光谱(h)及射频谱(i)[115]

Fig.10 Multi-wavelength mode-locking operation based the graphene topological insulator, and black phosphorus SA: (a) deposition setup of graphene by the evanescent light in tapered fiber; (b) optical microscope image of the GDTF; (c) the optical spectrum, and (d) the autocorrelation trace[105]; Reproduced with permission. Copyright 2012, IEEE photonics society; (e) the Raman spectrum (Inset: SEM of Bi_2Se_3); (f) the optical spectrum, and (g) the pulse train (Inset: single pulse)[111]; Reproduced with permission. Copyright 2014, SPIE; (g) Linear absorption spectrum and nonlinear transmission of BP. (h) Optical spectra, and (i) RF spectrum of dual-wavelength soliton pulses[115]; Reproduced with permission. Copyright 2014, Optical Society of America

后，基于石墨烯[106]和石墨烯氧化物[107]光纤器件的多波长锁模激光器也被研制出来。最近，为了避免光纤锥体的复杂制造技术，笔者课题组还发展了一种基于石墨烯三元复合膜的双波长孤子激光器[108]，如图11所示。值得注意的是，通过增加泵浦功率、优化光纤锥度参数和提高石墨烯的质量，可以进一步提高这些激光器的性能。需要指出的是，石墨烯作为锁模器表现出诸多优点，不过，也有两个不足：零带隙和弱吸收(单层吸收系数仅为 2.3%)，这严重限制了其光调制能力以及在强的光和物质相互作用领域中的

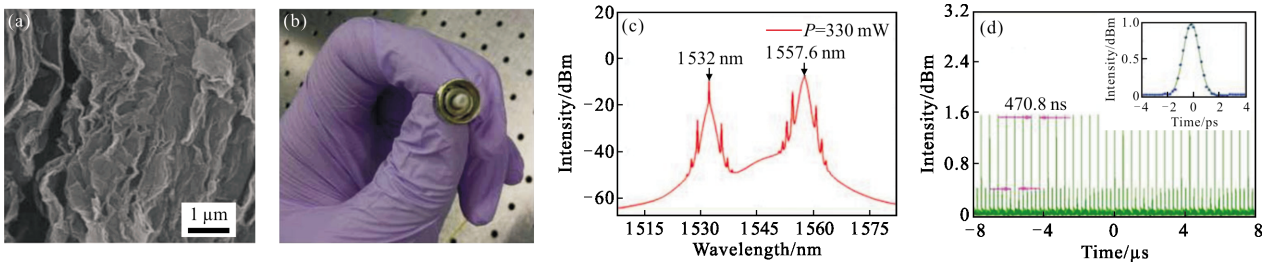

图 11 基于石墨烯三元复合薄膜的双波长孤子脉冲运转[108]：(a)G/SnO_2/PANI 薄膜的 SEM 照片；(b)粘贴石墨烯聚合物薄膜的光纤连接器端面照片；(c)光谱；(d)示波器迹(插图：自相关迹)

Fig.11 Dual-wavelength soliton pulse operation based on the graphene ternary composite film[108]: (a) the SEM morphology of G/SnO_2/PANI film; (b) the photograph of the surface of the fiber connecter with the graphene polymer film; (c) optical spectrum, and (d) the oscilloscope trace (inset: the autocorrelation trace). Reproduced with permission. Copyright 2017, Chinese Laser Press

应用。因此，探索新型材料成为国际上的热点问题。

除了石墨烯，其他类型的二维材料，例如：拓扑绝缘体[109-111]，过渡族金属硫化物[112-113]以及黑磷[114-115]，也被用于研制多波长超快激光器。例如，笔者课题组采用脉冲激光沉积法[112]和液相剥离法[113]制作的二硫化钨光纤拉锥器件，在掺铒光纤激光器中，首次实现了飞秒量级的双波长孤子脉冲运转。对于前者，获得了双波长孤子的最小脉冲宽度为 585 fs；对于后者，双波长孤子激光器的最大输出功率为 14.2 mW、最大脉冲能量为 6.63 nJ，如图 12 所示。研究表明，光纤激光器中双波长孤子脉冲的形成由腔内色散、双折射、高非线性和饱和吸收共同决定。此外，笔者课

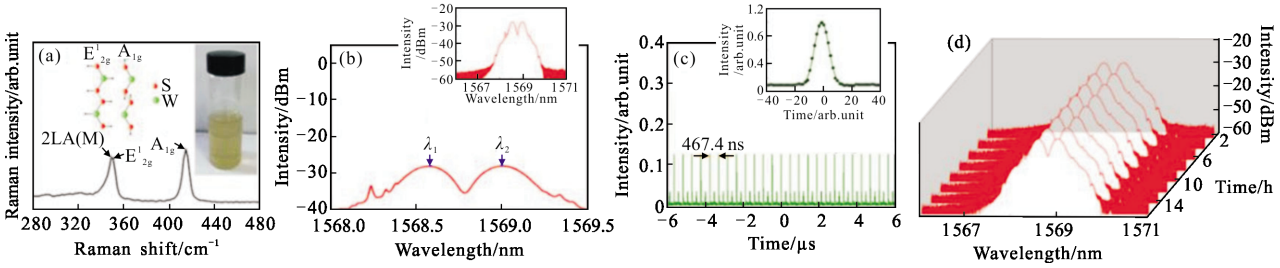

图 12 基于二硫化钨饱和吸收体的双波长孤子运转[113]:(a) WS_2 的拉曼光谱,插图:样品照片;(b)光谱;(c)示波器迹(插入:自相关迹)和(d)长期光谱

Fig.12 Dual-wavelength soliton operation based on the WS_2 SA[113]: (a) The Raman spectrum, inset: the photograph of WS_2 sample; (b) optical spectrum; (c) the oscilloscope trace (inset: the autocorrelation trace) and (d) long-term optical spectra. Reproduced with permission. Copyright 2018, Elsevier Science Press

题组还实现了基于拓扑绝缘体薄膜的可调谐三波长锁模运转,如图 10(d)~(f)所示。

近年来,研究发现,黑磷具有独特的结构和厚度依赖的直接带隙,在多波长超快激光领域有着十分诱人的前景[84-86]。例如,山东大学何京良课题组采用黑磷光纤器件,在掺铒光纤激光器中,获得了中心波长分别为 1533 nm 和 1558 nm 的双波长锁模脉冲运转[114]。此外,南京邮电大学云灵课题组利用少层黑磷作为可饱和吸收体,在掺铒光纤激光器中,获得了 1533~1558 nm 波段内,3 dB 带宽为 3.7~6.9 nm 的双波长偏振锁定矢量孤子脉冲[115],如图 10(g)~(i)所示。结果表明,少层黑磷作为饱和吸收体在多波长孤子脉冲产生中具有潜在的应用价值。

大量的研究表明,通过谐波锁模方式,激光器的脉冲重复率较腔的基本重复率有着显著增加。例如,华南师范大学信息与光电子学院罗智超课题组采用拓扑绝缘体沉积的拉锥光纤器件,在掺铒光纤激光器中,获得了重复率分别为 388 MHz 和 239 MHz 的双波长谐波锁模运转[116]。

在前述部分中,虽然国内外多个课题组已经实现了多波长超短脉冲的稳定输出,但这些脉冲运转于反常色散区域,属于传统孤子,其单脉冲能量较小,一般为亚纳焦量级,不能满足在激光微加工技术、激光测距以及光传感技术等领域的实际应用。为了解决这个问题,研究人员先后提出了几种方案:(1) 采用大模场面积的光纤,降低光纤非线性的影响,以实现高脉冲能量激光输出;(2) 利用啁啾脉冲放大技术,在腔外对脉冲进一步放大;(3) 设计腔内色散为正的光纤激光器,获得自相似脉冲或耗散孤子脉冲;其中,前两种方法需要进行严格的色散和非线性调控,导致激光器结构比较复杂。近年来的研究发现,耗散孤子脉冲是实现高脉冲能量的有效方式之一,它比传统孤子的单脉冲能量高几个数量级。研究发现,耗散孤子是通过腔内色散、克尔非线性、谱滤波效应和腔内损耗之间的非线性相互作用,在全正腔内色散条件下产生,其动力学过程由朗道-金兹堡方程描述。

近年来,采用二维材料光学器件,国内外多个课题组在光纤激光器中不仅获得了传统的耗散孤子,还实现了多波长耗散孤子运转。例如,厦门大学电子工程系罗正钱课题组利用石墨烯沉积的拉锥器件,在掺铒光纤激光器中,实现了脉冲宽度为 74.6 ps、脉冲能量为 6.4 nJ 的三波长耗散孤子运转[117],如图 13(a)~(d)所示。研究发现,由于石墨烯与锥体之间的倏逝场相互作用,该器件具有饱和吸收和偏振效应两种特性,使之不仅能够启动基于饱和吸收的锁模运转,而且还可以诱导特殊的频谱滤波和非线性偏振演化,将腔内脉冲整形成多波长耗散孤子脉冲。与石墨烯不同,氧化石墨烯具有水溶性,这为其实际应用提供了更多选择。例如,深圳大学激光工程重点实验室闫培光课题组利用氧化石墨烯器件,在掺镱光纤激光器中,实现了可调谐、可切换的双波长和三波长耗散孤子运转[118],如图 13(e)~(g)所示。这些简单、紧凑和全光纤化的多波长耗散孤子光纤激光器有着许多潜在的应用前景。

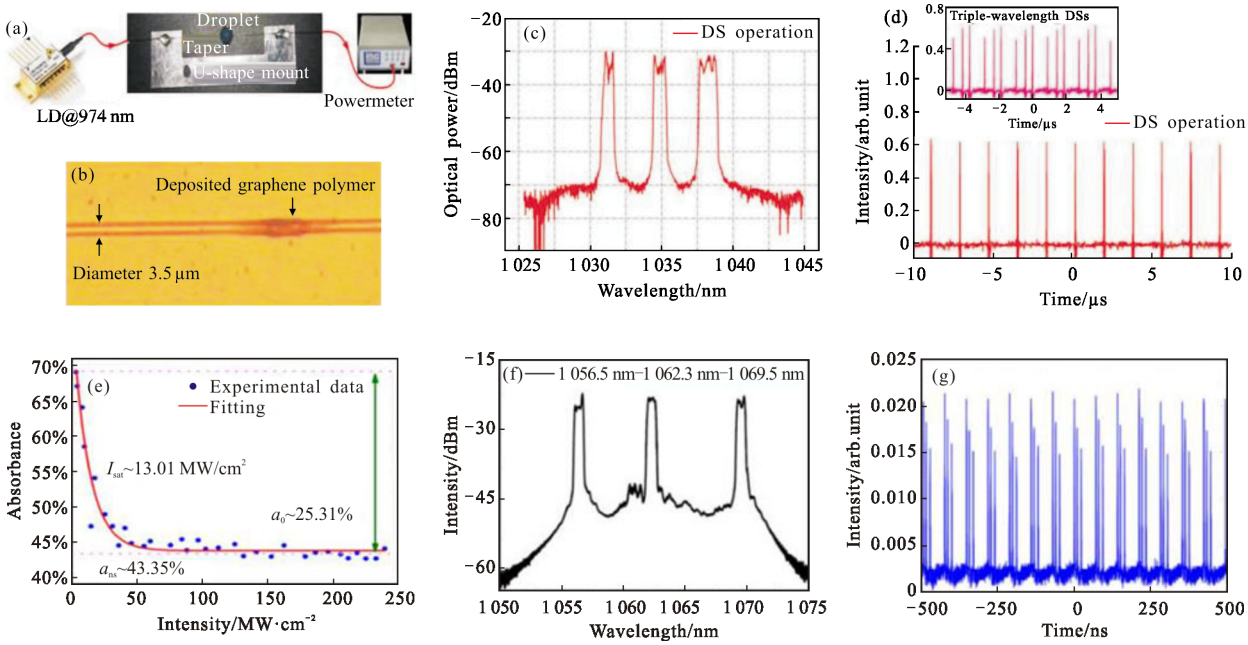

图 13 基于石墨烯和氧化石墨烯的三波长耗散孤子运转:(a)利用倏逝光在锥形光纤中沉积石墨烯的实验装置;(b)石墨烯拉锥器件的光学显微镜照片;(c)光谱和(d)脉冲串[87];(e)氧化石墨烯器件的饱和吸收曲线;(f)光谱;(g)脉冲序列[118]

Fig.13 Triple-wavelength DS operation based the graphene and GO SA: (a) Deposition setup of graphene by the evanescent light in tapered fiber; (b) optical microscope image of the GDTF; (c) the optical spectrum; (d) the pulse train[117]. Reproduced with permission. Copyright 2012, IEEE photonics society; (e) the saturable absorption curve; (f) the optical spectrum; (g) the pulse train[118]. Reproduced with permission. Copyright 2014, Optical Society of America

近年来的研究发现，矩形脉冲也是实现高脉冲能量的有效方式之一。矩形脉冲光纤激光器因其在光通信、光谱学、传感研究、激光微加工、烧蚀等领域的广泛应用而具有重要的应用价值。研究人员利用主动或被动锁模技术在光纤激光器中获得了矩形脉冲。有趣的是，除了单波长运转，利用二维材料光学器件，还实现了多波长矩形脉冲运转。2015 年，笔者课题组利用拓扑绝缘体的双重特性，在掺铒光纤激光器反常色散区，实现了双波长矩形脉冲输出[119]，如图 14(a)~(c)所示，其脉冲宽度为 13.62~25.16 ns，对应的脉冲能量为 0.593~2.824 nJ，远高于传统孤子脉冲能量(<0.1 nJ)。除了基频运转，还进一步地实现了双波长矩形脉冲的高次谐波运转。此外，华南师范大学信息与光电子学院罗智超课题组采用石墨烯沉积的拉锥光学器件，在掺镱光纤激光器中，获得了双波长矩形脉冲[120]，如图 14(d)~(f)所示。研究发现，随着泵浦功率的增加，该双波长矩形脉冲的脉冲宽度可以从 1.41 ns 线性增加到 4.23 ns。进而，利用可调谐带通滤波器，他们发现，两个以 1 061.8 nm 和 1 068.8 nm 为中心的矩形脉冲的特性相似。此外，重庆大学朱涛课题组利用还原氧化石墨烯，在掺铒光纤激光器中，观察到矢量型的双波长矩形脉冲输出[121]。这些研究表

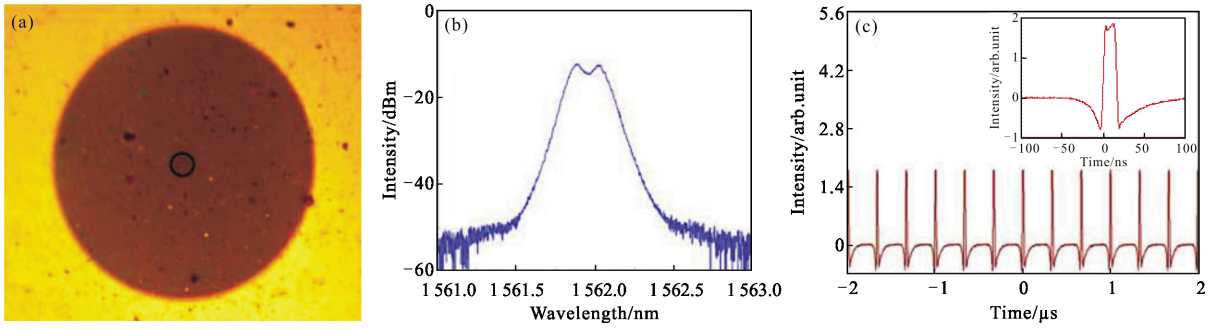

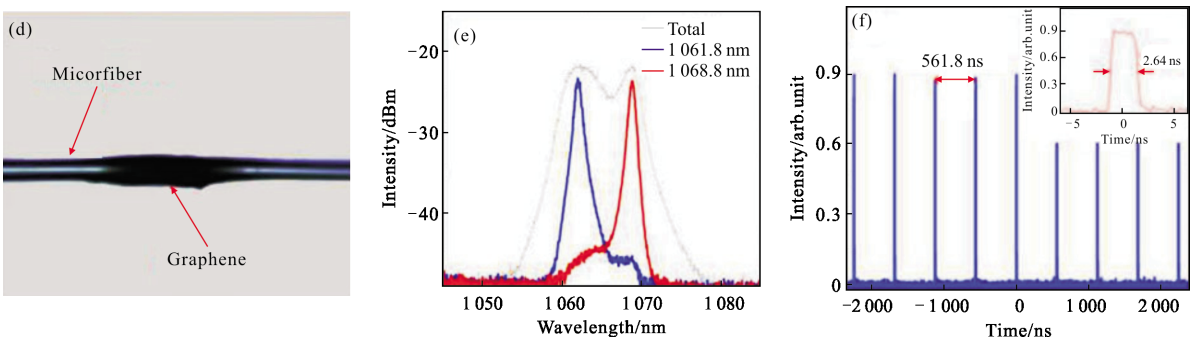

图 14 基于 Bi_2Se_3 和石墨烯的双波长矩形脉冲运转：(a)粘贴 Bi_2Se_3 聚合物薄膜的光纤连接器端面照片；(b)光谱；(c)脉冲串(插图：单脉冲)[119]；(d)制备的基于石墨烯饱和吸收体的显微照片；(e)光谱；(f)脉冲序列(插图：单脉冲[120])

Fig.14 Dual-wavelength rectangular pulse operation based on few-layer Bi_2Se_3[119] and graphene[120]: (a) the photograph of the surface of the fiber connecter with the Bi_2Se_3 polymer film; (b) the optical spectrum; (c) pulse-train. Inset: single pulse. Reproduced with permission. Copyright 2015, Optical Society of America. (d) the microscopy image of fabricated microfiber-based GSA; (e) optical spectrum; (f) pulse-train. Inset: single pulse. Reproduced with permission. Copyright 2014, Optical Society of America

明，多波长矩形脉冲光纤激光器具有十分灵活的脉冲特性，为其在高脉冲能量领域的应用开辟了新的途径。

有趣的是，其他方案也得到发展。采用氧化石墨烯饱和吸收体，聊城大学张丙元课题组还实现了脉冲宽度为 441 ps、重复频率为 100 MHz、最大平均输出功率为 189 mW 的双波长被动调 Q 锁模 Nd:GYSGG 激光器[122]。

自 1996 年 Vengsakar 首次成功制备以来，长周期光栅已成为当前光纤领域的研究热点之一[123]。超长周期光栅，其在轴向上的有效折射率在光纤中以毫米量级的周期性调制，传播光在一定的谐振波长下基模和包层模之间耦合。2003 年，Intrachat 和 Kutz 在理论上提出了超长周期光栅的脉冲整形理论，当连续波在腔内传播多次往返时，利用超长周期光栅，可以实现锁模[124-125]。最近，研究发现，超长周期光栅具有双重功能，即锁模器和多波长滤波器。进而，在掺铒光纤激光器中，实现了三波长到七波长级联锁模运转[126]，如图 15 所示。

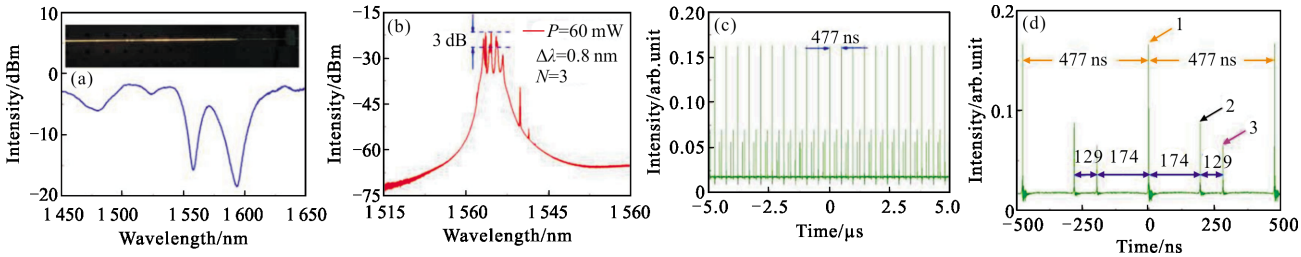

图 15 基于超长周期光栅器件的三波长孤子运转[126]：(a)透射光谱(插图：可见光透射时的照片)；(b)光谱；(c)脉冲序列和(d)相应的脉冲放大图片

Fig.15 Triple-wavelength soliton operation based on the ULPG device[126]: (a) the transmission spectrum (Inset: the photograph when the visible light transmitting); (b) the optical spectrum; (c) the pulse train; (d) its corresponding zoom-in image

4.2 多波长光学现象

被动锁模光纤激光器是研究光孤子演化动力学和非线性现象的一个很好平台，近年来受到了广泛关注。研究发现，在锁模激光器参数中，高非线性对腔内多孤子的产生和演化至关重要。如前所述，除了饱和吸收效应之外，二维材料还表现出一个很大的非线性折射率，如表 1 所示。进而，若将二维材料转移到光纤器件上，还可以有效地增加光和二维材料之间的相互作用长度。因此，将之转移至光纤激光器中，使得它非常适合于研究非线性光学现象。

1974，Manakov 利用耦合非线性薛定谔方程从理论上研究了光脉冲在高双折射光纤中的传播特

性[127]。他们指出，慢轴上的暗脉冲和快轴上的亮脉冲可以同时不失真地长时间传播。因此，可能存在暗-暗、亮-亮、甚至暗-亮孤子对。然而，直到现在为止，它们在实验中较少被观察到。利用 Bi_2Se_3 聚合物薄膜，在掺铒光纤激光器中，笔者观察到了双波长亮-暗孤子对[128-129]。对于亮-暗孤子对，发现它的整个光谱中包含两个不同的部分：一个是位于较短波长处的亮孤子，另一个是位于较长波长处的双波长暗孤子，如图 16(a)~(c)所示。进而，我们还实现了亮-暗孤子对的谐波锁模，其最高重复频率约为 433.8 MHz，相当于基本重复频率的 280 次谐波。此外，还观察到了双波长台阶-暗孤子混合型脉冲[129]。

最近，北京工业大学宋晏蓉课题组利用 Bi_2Se_3 聚乙烯醇薄膜，在掺铒光纤激光器中，实现了波长可切换的双波长孤子运转[130]，如图 16(d)~(f)所示。通过偏振控制器和泵浦功率的适当设置，观察到了一种新型双波长孤子脉冲。该双波长脉冲可工作在两个不同的锁模状态。一个是在 1532 nm 处的单脉冲锁模，

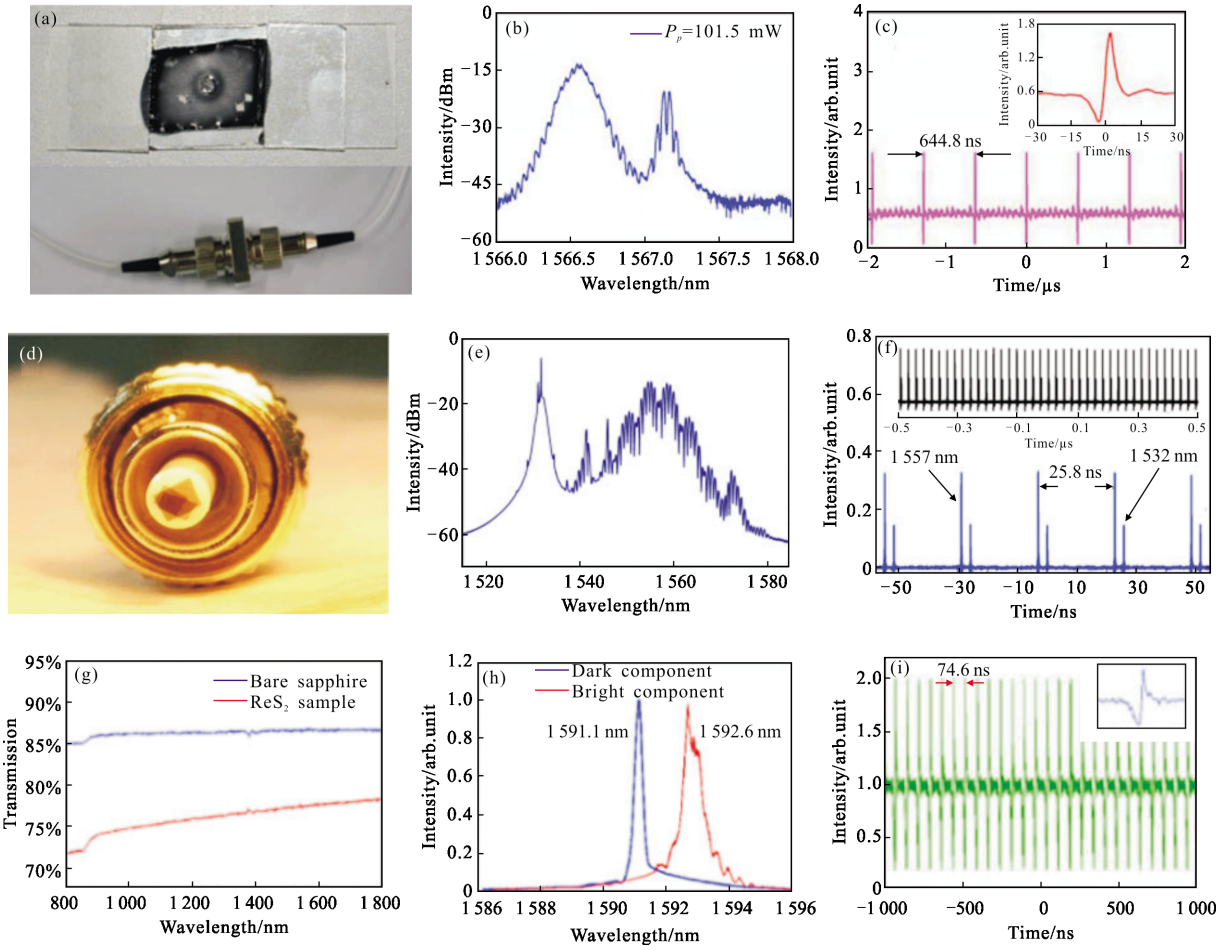

图 16 基于 Bi_2Se_3 和 ReS_2 饱和吸收体的双波长亮-暗孤子对和束缚态运转：(a)Bi_2Se_3 聚合物薄膜及锁模器照片；(b)输出光谱；(c)脉冲序列(插图：放大单脉冲分布)[129]；(d)粘贴 Bi_2Se_3 聚合物薄膜的光纤连接器端面照片；(e)光谱；(f)相应的脉冲序列[130]；(g)与裸蓝宝石相比，ReS_2 样品的线性透过率；(h)亮脉冲和暗脉冲的输出光谱；(i)典型的脉冲序列(插图：相应的单脉冲分布[131])

Fig.16 Dual-wavelength bright-dark soliton pair operation based on the Bi_2Se_3 SA: the photograph of the Bi_2Se_3 polymer film (a) and the mode-locker; (b) the output optical spectrum; (c) the pulse train (inset: the zoom-in single pulse profile)[129], Reproduced with permission. Copyright 2016, IEEE photonics society; (d) the photograph of the surface of the fiber connecter with the Bi_2Se_3 polymer film; (e) the optical spectrum; (f) the corresponding pulse train[130]; Reproduced with permission. Copyright 2017, IEEE photonics society; (g) Linear transmittance of ReS_2-sample in comparison with bare sapphire; (h) output spectrum of the bright pulse and the dark pulse; (i) Typical pulse train. The inset shows the corresponding single pulse profile[131]; Reproduced with permission. Copyright 2014, Optical Society of America

另一个是在 1557 nm 处的束缚孤子态。此外,山东大学何京良课题组利用 ReS_2 饱和吸收体,在光纤激光器中,还观察到多波长亮-暗脉冲对[131],如图 16(g)~(i)所示。这些结果表明,二维材料既可作为短脉冲产生的优良饱和吸收体,又可以作为高非线性光子学材料。

5 结论及展望

文中回顾了基于二维材料的多波长超快激光器及相关的非线性光学现象,并讨论了二维材料的制备和非线性光学性质。从未来发展的角度来看,可以从四个方面来进一步改善基于二维材料的多波长激光器性能。

更高的脉冲能量 希望通过优化激光腔的设计,提高二维材料的质量,或者在未来的研究中插入高质量的梳状滤波器,进一步提高所提出的多波长锁模光纤激光器的质量和脉冲能量。

更宽的运转波长范围 被动锁模由于其简单的结构,已成为获得超快中红外脉冲的理想选择。可以预期,基于二维材料的中红外多波长脉冲也可以被实现。

更丰富的非线性光学现象 可以预期,在未来的工作中,也可以通过使用基于二维材料的激光器来观测更多的孤子脉冲类型,如:相似子、耗散孤子共振和多孤子分子。

更多的二维材料类型 石墨烯相关的二维晶体和杂化材料现在正从纯科学迅速发展为技术应用。在不久的将来,其他的二维材料将在超快光子学领域得到发展。

二维材料作为近年来最重要的研究热点之一,将在不久的将来,提高对人类社会的认识和影响。笔者期待在未来的若干年里,基于二维材料非线性光学器件的多波长超快激光器获得快速发展。

参考文献:

[1] Keller U. Recent developments in compact ultrafast lasers[J]. Nature, 2003, 424(6950): 831.

[2] Suh M G, Yang Q F, Yang K Y, et al. Microresonator soliton dual-combspectroscopy [J]. Science, 2016, 354(6312): 600-613.

[3] Li J, Yi X, Lee H, et al. Electro-optical frequency division and stablemicrowave synthesis [J]. Science, 2014, 345(6194): 309-313.

[4] Agrawal G P. Nonlinear Fiber Optics [M]. Berlin: Springer, 2000: 195-211.

[5] Schlager J B, Kawanishi S, Saruwatari M. Dual wavelength pulse generation using mode-locked erbium-doped fibre ring laser [J]. Electronics Letters, 1991, 27(22): 2072-2073.

[6] Li S, Chan K T. Electrical wavelength tunable and multiwavelength actively mode-locked fiber ring laser [J]. Applied Physics Letters, 1998, 72(16): 1954-1956.

[7] Zhao Y, Shu C. A fiber laser for effective generation of tunable single- and dual-wavelength mode-locked optical pulses[J]. Applied Physics Letters, 1998, 72(13): 1556-1558.

[8] Bakhshi B, Andrekson P A. Dual-wavelength 10-GHz actively mode-locked erbium fiber laser [J]. IEEE Photonics Technology Letters, 1999, 11(11): 1387-1389.

[9] Deparis O, Kiyan R, Salik E, et al. Round-trip time and dispersion optimization in a dual-wavelength actively mode-locked Er-doped fiber laser including nonchirped fiber Bragg gratings [J]. IEEE Photonics Technology Letters, 1999, 11(10): 1238-1240.

[10] Town G E, Chen L, Smith P W E. Dual-wavelength mode-locked fiber laser [J]. IEEE Photonics Technology Letters, 2000, 12(11): 1459-1461.

[11] Pudo D, Chen L R. Actively mode-locked, quadruple-wavelength fibre laser with pump-controlled wavelength switching [J]. Electronics Letters, 2003, 39(3): 272-274.

[12] Lou J W, Carruthers T F, Currie M. 4×10 GHz mode-locked multiple-wavelength fiber laser [J]. IEEE Photonics Technology Letters, 2004, 16(1): 51-53.

[13] Yao J, Yao J, Deng Z. Multiwavelength actively mode-locked fiber ring laser with suppressed homogeneous line broadening and reduced supermodenoise [J]. Optics Express, 2004, 12(19): 4529-4534.

[14] Chen Z, Ma S, Dutta N K. Multiwavelength fiber ring laser based on a semiconductor and fiber gain medium [J]. Optics Express, 2009, 17(3): 1234-1239.

[15] Noske D U, Guy M J, Rottwitt K, et al. Dual-wavelength operation of a passively mode-locked "figure-of-eight" ytterbium-erbium fibre soliton laser [J]. Optics Communications, 1994, 108(4-6): 297-301.

[16] Yun L, Liu X, Mao D. Observation of dual-wavelength dissipative solitons in a figure-eight erbium-doped fiber laser [J]. Optics Express, 2012, 20(19): 20992-20997.

[17] Ning Q Y, Wang S K, Luo A P, et al. Bright-dark pulse

pair in a figure-eight dispersion-managed passively mode-locked fiber laser [J]. IEEE Photonics Journal, 2012, 4(5): 1647-1652.

[18] Krzempek K, Sobon G, Sotor J, et al. Fully-integrated dual-wavelength all-fiber source for mode-locked square-shaped mid-IR pulse generation via DFG in PPLN [J]. Optics Express, 2015, 23(25): 32080-32086.

[19] Jin X, Wang X, Wang X, et al. Tunable multiwavelength mode-locked Tm/Ho-doped fiber laser based on a nonlinear amplified loop mirror [J]. Applied Optics, 2015, 54(28): 8260-8264.

[20] Shao Z, Qiao X, Rong Q, et al. Generation of dual-wavelength square pulse in a figure-eight erbium-doped fiber laser with ultra-large net-anomalous dispersion [J]. Applied Optics, 2015, 54(22): 6711-6716.

[21] Posada-Ramírez B, Durán-Sánchez M, Álvarez-Tamayo R I, et al. Study of a Hi-Bi FOLM for tunable and dual-wavelength operation of a thulium-doped fiber laser [J]. Optics Express, 2017, 25(3): 2560-2568.

[22] Matsas V J, Newson T P, Richardson D J, et al. Selfstarting passively mode-locked fibre ring soliton laser exploiting nonlinear polarisation rotation [J]. Electronics Letters, 1992, 28(15): 1391-1393.

[23] Gong Y D, Tian X L, Tang M, et al. Generation of dual wavelength ultrashort pulse outputs from a passive mode locked fiber ring laser [J]. Optics Communications, 2006, 265(2): 628-631.

[24] Zhang Z, Zhan L, Xu K, et al. Multiwavelength fiber laser with fine adjustment, based on nonlinear polarization rotation and birefringence fiber filter[J]. Optics Letters, 2008, 33(4): 324-326.

[25] Chen Z, Sun H, Ma S, et al. Dual-wavelength mode-locked erbium-doped fiber ring laser using highly nonlinear fiber [J]. IEEE Photonics Technology Letters, 2008, 20(24): 2066-2068.

[26] Chen W C, Luo Z C, Xu W C. The interaction of dual wavelength solitons in fiber laser [J]. Laser Physics Letters, 2009, 6(11): 816.

[27] Luo Z C, Luo A P, Xu W C, et al. Modulation instability induced by cross-phase modulation in a dual-wavelength dispersion-managed soliton fiber ring laser[J]. Applied Physics B, 2010, 100(4): 811-820.

[28] Luo Z C, Luo A P, Xu W C, et al. Tunable multiwavelength passively mode-locked fiber ring laser using intracavity birefringence-induced comb filter [J]. IEEE Photonics Journal, 2010, 2(4): 571-577.

[29] Luo A P, Luo Z C, Xu W C, et al. Tunable and switchable dual-wavelength passively mode-locked Bi-doped all-fiber ring laser based on nonlinear polarization rotation [J]. Laser Physics Letters, 2011, 8(8): 601-605.

[30] Zhu X, Wang C, Liu S, et al. Switchable dual-wavelength and passively mode-locked all-normal-dispersion Yb-doped fiber lasers [J]. IEEE Photonics Technology Letters, 2011, 23(14): 956-958.

[31] Mao D, Liu X, Wang L, et al. Dual-wavelength step-like pulses in an ultra-large negative-dispersion fiber laser [J]. Optics Express, 2011, 19(5): 3996-4001.

[32] Zhang H, Tang D, Zhao L, et al. Dual-wavelength domain wall solitons in a fiber ring laser [J]. Optics Express, 2011, 19(4): 3525-3530.

[33] Yun L, Han D. Evolution of dual-wavelength fiber laser from continuous wave to soliton pulses [J]. Optics Communications, 2012, 285(24): 5406-5409.

[34] Zhang Z X, Xu Z W, Zhang L, et al. Tunable and switchable dual-wavelength dissipative soliton generation in an all-normal-dispersion Yb-doped fiber laser with birefringence fiber filter [J]. Optics Express, 2012, 20(24): 26736-26742.

[35] Mao D, Lu H. Formation and evolution of passively mode-locked fiber soliton lasers operating in a dual-wavelength regime [J]. Journal of The Optical Society of America B-Optical Physics, 2012, 29(10): 2819-2826.

[36] Lin H, Guo C, Ruan S, et al. Tunable and switchable dual-wavelength dissipative soliton operation of a weak-birefringence all-normal-dispersion Yb-doped fiber laser [J]. IEEE Photonics Journal, 2013, 5(5): 1501807-1501807.

[37] Wang X, Zhu Y, Zhou P, et al. Tunable, multiwavelength Tm-doped fiber laser based on polarization rotation and four-wave-mixing effect [J]. Optics Express, 2013, 21(22): 25977-25984.

[38] Yan Z, Li X, Tang Y, et al. Tunable and switchable dual-wavelength Tm-doped mode-locked fiber laser by nonlinear polarization evolution [J]. Optics Express, 2015, 23(4): 4369-4376.

[39] Yan Z, Tang Y, Sun B, et al. Switchable multi-wavelength Tm-doped mode-locked fiber laser [J]. Optics Letters, 2015, 40(9): 1916-1919.

[40] Zhang Z, Mou C, Yan Z, et al. Switchable dual-wavelength Q-switched and mode-locked fiber lasers using a large-angle tilted fiber grating [J]. Optics Express, 2015, 23(2): 1353-1360.

[41] Wang S, Zhao Z, Kobayashi Y, et al. Wavelength-spacing controllable, dual-wavelength synchronously mode locked Er: fiber laser oscillator based on dual-branch nonlinear polarization rotation technique [J]. Optics Express, 2016, 24 (25): 28228-28238.

[42] Feehan J S, Ilday F O, Brocklesby W S, et al. Simulations and experiments showing the origin of multi-wavelength mode locking in femtosecond, Yb-fiber lasers [J]. Journal of The Optical Society of America B-Optical Physics, 2016, 33(8): 1668-1676.

[43] Zhang H, Tang D Y, Wu X, et al. Multi-wavelength dissipative soliton operation of an erbium-doped fiber laser [J]. Optics Express, 2009, 17(15): 12692-12697.

[44] Luo Z, Luo A, Xu W, et al. Tunable and switchable multiwavelength passively mode-locked fiber laser based on SESAM and inline birefringence comb filter [J]. IEEE Photonics Journal, 2011, 3(1): 64-70.

[45] Luo A P, Luo Z, Xu W C, et al. Switchable dual-wavelength passively mode-locked fiber ring laser using SESAM and cascaded fiber Bragg gratings [J]. Laser Physics, 2011, 21 (2): 395-398.

[46] Li J, Luo H, Wang L, et al. Mid-infrared passively switched pulsed dual wavelength Ho^{3+}-doped fluoride fiber laser at 3 μm and 2 μm [J]. Scientific Reports, 2015, 5(1): 10770-10770.

[47] Rigaud P, Kermene V, Simos C, et al. Dual-wavelength synchronous ultrashort pulses from a mode-locked Yb-doped multicore fiber laser with spatially dispersed gain [J]. Optics Express, 2015, 23(19): 25308-25315.

[48] Wu Z, Fu S, Chen C, et al. Dual-state dissipative solitons from an all-normal-dispersion erbium-doped fiber laser: continuous wavelength tuning and multi-wavelength emission [J]. Optics Letters, 2015, 40(12): 2684-2687.

[49] Zhang Y, Yang C, Feng Z, et al. Dual-wavelength passively Q-switched single-frequency fiber laser [J]. Optics Express, 2016, 24(14): 16149-16155.

[50] Waritanant T, Major A. Discretely selectable multiwavelength operation of a semiconductor saturable absorber mirror mode-locked Nd:YVO_4 laser [J]. Optics Letters, 2017, 42 (17): 3331-3334.

[51] Li J, Wang Y, Zhang E, et al. Coexistence of noise-like pulse and high repetition rate harmonic mode-locking in a dual-wavelength mode-locked Tm-doped fiber laser [J]. Optics Express, 2017, 25(15): 17992-17200.

[52] Zhao X, Zheng Z, Liu L, et al. Switchable, dual-wavelength passively mode-locked ultrafast fiber laser based on a single-wall carbon nanotube mode-locker and intracavity loss tuning [J]. Optics Express, 2011, 19(2): 1168-1173.

[53] Zhao X, Zheng Z, Liu L, et al. Fast, long-scan-range pump-probe measurement based on asynchronous sampling using a dual-wavelength mode-locked fiber laser [J]. Optics Express, 2012, 20(23): 25584-25589.

[54] Liu X, Han D, Sun Z, et al. Versatile multi-wavelength ultrafast fiber laser mode-locked by carbon nanotubes [J]. Scientific Reports, 2013, 3(1): 2718-2718.

[55] Chen G W, Li W L, Yang H R, et al. Switchable dual-wavelength fiber laser mode-locked by carbon nanotubes [J]. Journal of Modern Optics, 2015, 62(5): 353-357.

[56] Jiang K, Wu Z, Fu S, et al. Switchable dual-wavelength mode-locking of thulium-doped fiber laser Based on SWNTs [J]. IEEE Photonics Technology Letters, 2016, 28 (19): 2019-2022.

[57] Geim A K. Graphene: status and prospects [J]. Science, 2009, 324(5934): 1530-1534.

[58] Zhang H. Ultrathin two-dimensional nanomaterials [J]. ACS Nano, 2015, 9(10): 9451-9469.

[59] Coleman J N, Lotya M, O'Neill A, et al. Two-dimensional nanosheets produced by liquid exfoliation of layered materials [J]. Science, 2011, 331(6017): 568-571.

[60] Nicolosi V, Chhowalla M, Kanatzidis M G, et al. Liquid exfoliation of layered materials [J]. Science, 2013, 340 (6139): 1226419.

[61] Bao Q, Zhang H, Wang Y, et al. Atomic-layer graphene as a saturable absorber for ultrafast pulsed lasers [J]. Advanced Functional Materials, 2009, 19(19): 3077-3083.

[62] Bonaccorso F, Sun Z, Hasan T, et al. Graphene photonics and optoelectronics [J]. Nature Photonics, 2010, 4(9): 611-622.

[63] Xia F, Wang H, Xiao D, et al. Two-dimensional material nanophotonics [J]. Nature Photonics, 2014, 8(12): 899-907.

[64] Zhang H, Lu S, Zheng J, et al. Molybdenum disulfide (MoS_2) as a broadband saturable absorber for ultra-fast photonics[J]. Optics Express, 2014, 22(6): 7249-7260.

[65] Sobon G. Mode-locking of fiber lasers using novel two-dimensional nanomaterials: graphene and topological insulators [J]. Photonics Research, 2015, 3(2): A56-A63.

[66] Yu S, Wu X, Wang Y, et al. 2D Materials for optical modulation: challenges and opportunities [J]. Advanced Materials, 2017, 29(14): 1606128.

[67] Liu X, Guo Q, Qiu J. Emerging low-dimensional materials

for nonlinear optics and ultrafast photonics [J]. Advanced Materials, 2017, 29(14): 1605886.

[68] Guo B. 2D noncarbon materials-based nonlinear optical devices for ultrafast photonics [J]. Chinese Optics Letters, 2018, 16(2): 020004.

[69] Liu Z, Wang Y, Zhang X, et al. Nonlinear optical properties of graphene oxide in nanosecond and picosecond regimes [J]. Applied Physics Letters, 2009, 94(2): 021902.

[70] Hendry E, Hale P J, Moger J, et al. Coherent nonlinear optical response of graphene [J]. Physical Review Letters, 2010, 105(9): 097401.

[71] Hsieh D, Qian D, Wray L, et al. A topological Dirac insulator in a quantum spin Hall phase [J]. Nature, 2008, 452(7190): 970.

[72] Chen Y L, Analytis J G, Chu J H, et al. Experimental realization of a three-dimensional topological insulator, Bi_2Te_3 [J]. Science, 2009, 325(5937): 178-181.

[73] Xia Y, Qian D, Hsieh D, et al. Observation of a large-gap topological-insulator class with a single Dirac cone on the surface [J]. Nature Physics, 2009, 5(6): 398.

[74] Zhang Y, He K, Chang C Z, et al. Crossover of the three-dimensional topological insulator Bi_2Se_3 to the two-dimensional limit [J]. Nature Physics, 2010, 6(8): 584.

[75] Moore J E. The birth of topological insulators [J]. Nature, 2010, 464(7286): 194.

[76] Hasan M Z, Kane C L. Colloquium: topological insulators [J]. Reviews of Modern Physics, 2010, 82(4): 3045.

[77] Qi X L, Zhang S C. Topological insulators and superconductors [J]. Reviews of Modern Physics, 2011, 83(4): 1057.

[78] Bernard F, Zhang H, Gorza S P, et al. Towards mode-locked fiber laser using topological insulators [C]//Nonlinear Photonics. Optical Society of America, 2012: NTh1A. 5.

[79] Lu S, Zhao C, Zou Y, et al. Third order nonlinear optical property of Bi_2Se_3 [J]. Optics Express, 2013, 21(2): 2072-2082.

[80] Chen S, Zhao C, Li Y, et al. Broadband optical and microwave nonlinear response in topological insulator [J]. Optical Materials Express, 2014, 4(4): 587-596.

[81] Wang Q H, Kalantar-Zadeh K, Kis A, et al. Electronics and optoelectronics of two-dimensional transition metal dichalcogenides [J]. Nature Nanotechnology, 2012, 7(11): 699.

[82] Wang K, Wang J, Fan J, et al. Ultrafast saturable absorption of two-dimensional MoS_2 nanosheets [J]. ACS Nano, 2013, 7(10): 9260-9267.

[83] Sun J, Gu Y J, Lei D Y, et al. Mechanistic understanding of excitation-correlated nonlinear optical properties in MoS_2 nanosheets and nanodots: the role of exciton resonance [J]. ACS Photonics, 2016, 3(12): 2434-2444.

[84] Ling X, Wang H, Huang S, et al. The renaissance of black phosphorus [J]. Proceedings of the National Academy of Sciences, 2015: 201416581.

[85] Wang X, Lan S. Optical properties of black phosphorus [J]. Advances in Optics and Photonics, 2016, 8(4): 618-655.

[86] Dhanabalan S C, Ponraj J S, Guo Z, et al. Emerging trends in phosphorene fabrication towards next generation devices [J]. Advanced Science, 2017, 4(6): 1600305.

[87] Lu S B, Miao L L, Guo Z N, et al. Broadband nonlinear optical response in multi-layer black phosphorus: an emerging infrared and mid-infrared optical material [J]. Optics Express, 2015, 23(9): 11183-11194.

[88] Martinez A, Sun Z. Nanotube and graphene saturable absorbers for fibre lasers [J]. Nature Photonics, 2013, 7(11): 842.

[89] Luo Z, Zhou M, Weng J, et al. Graphene-based passively Q-switched dual-wavelength erbium-doped fiber laser [J]. Optics Letters, 2010, 35(21): 3709-3711.

[90] Luo Z, Zhou M, Wu D, et al. Graphene-induced nonlinear four-wave-mixing and its application to multiwavelength Q-switched rare-earth-doped fiber lasers [J]. Journal of Lightwave Technology, 2011, 29(18): 2732-2739.

[91] Wang Z T, Chen Y, Zhao C J, et al. Switchable dual-wavelength synchronously Q-switched erbium-doped fiber laser based on graphene saturable absorber [J]. IEEE Photonics Journal, 2012, 4(3): 869-876.

[92] Ahmad H, Zulkifli M Z, Muhammad F D, et al. Passively Q-switched 11-channel stable brillouin erbium-doped fiber laser with graphene as the saturable absorber [J]. IEEE Photonics Journal, 2012, 4(5): 2050-2056.

[93] Zhao J, Wang Y, Yan P, et al. Graphene-oxide-based Q-switched fiber laser with stable five-wavelength operation[J]. Chinese Physics Letters, 2012, 29(11): 114206.

[94] Lou F, Zhao R, He J, et al. Nanosecond-pulsed, dual-wavelength, passively Q-switched ytterbium-doped bulk laser based on few-layer MoS_2 saturable absorber [J]. Photonics Research, 2015, 3(2): A25-A29.

[95] Gao Y J, Zhang B Y, Song Q, et al. Dual-wavelength passively Q-switched Nd: GYSGG laser by tungsten disulfide saturable absorber[J]. Applied Optics, 2016, 55(18): 4929-4932.

[96] Zhang H, He J, Wang Z, et al. Dual-wavelength, passively

Q-switched Tm: YAP laser with black phosphorus saturable absorber [J]. Optical Materials Express, 2016, 6 (7): 2328-2335.

[97] Zhao Y, Li X, Xu M, et al. Dual-wavelength synchronously Q-switched solid-state laser with multi-layered graphene as saturable absorber[J]. Optics Express, 2013, 21(3): 3516-3522.

[98] Wang B, Yu H, Zhang H, et al. Topological insulator simultaneously Q-switched dual-wavelength Nd:Lu_2O_3 laser [J]. IEEE Photonics Journal, 2014, 6(3): 1-7.

[99] Lou F, Zhao R, He J, et al. Nanosecond-pulsed, dual-wavelength, passively Q-switched ytterbium-doped bulk laser based on few-layer MoS_2 saturable absorber [J]. Photonics Research, 2015, 3(2): A25-A29.

[100] Guo J, Zhang H, Li P. Graphene Q-switched eye-safe Nd: $Y_3Al_5O_{12}$ ceramic dual-wavelength laser [J]. Applied Optics, 2015, 54(22): 6694-6697.

[101] Chu H, Zhao S, Li T, et al. Dual-wavelength passively Q-switched Nd, Mg: $LiTaO_3$ laser with a monolayer graphene as saturable absorber [J]. IEEE Journal of Selected Topics in Quantum Electronics, 2015, 21(1): 343-347.

[102] Sun Y J, Lee C K, Xu J L, et al. Passively Q-switched tri-wavelength Yb^{3+}: $GdAl_3$ $(BO_3)_4$ solid-state laser with topological insulator Bi_2Te_3 as saturable absorber [J]. Photonics Research, 2015, 3(3): A97-A101.

[103] Liu J, Liu J, Guo Z, et al. Dual-wavelength Q-switched Er: SrF_2 laser with a black phosphorus absorber in the mid-infrared region [J]. Optics Express, 2016, 24 (26): 30289-30295.

[104] Zhang H, He J, Wang Z, et al. Dual-wavelength, passively Q-switched Tm: YAP laser with black phosphorus saturable absorber[J]. Optical Materials Express, 2016, 6(7): 2328-2335.

[105] Luo Z Q, Wang J Z, Zhou M, et al. Multiwavelength mode-locked erbium-doped fiber laser based on the interaction of graphene and fiber-taper evanescent field [J]. Laser Physics Letters, 2012, 9(3): 229.

[106] Lau K Y, Bakar M H A, Muhammad F D, et al. Dual-wavelength, mode-locked erbium-doped fiber laser employing a graphene/polymethyl-methacrylate saturable absorber[J]. Optics Express, 2018, 26(10): 12790-12800.

[107] Zhao J, Wang Y, Ruan S, et al. Three operation regimes with an L-band ultrafast fiber laser passively mode-locked by graphene oxide saturable absorber [J]. JOSA B, 2014, 31 (4): 716-722.

[108] Guo B, Ouyang Q, Li S, et al. Dual-wavelength soliton laser based on the graphene ternary composite [J]. Chinese Journal of Lasers, 2017, 44(7): 0703012.

[109] Guo B, Yao Y, Yang Y F, et al. Topological insulator: Bi_2Se_3/polyvinyl alcohol film-assisted multi-wavelength ultrafast erbium-doped fiber laser [J]. Journal of Applied Physics, 2015, 117(6): 063108.

[110] Guo B, Yao Y, Yang Y F, et al. Tunable multi-wavelength mode-locked fiber laser with topological insulator: Bi_2Se_3/PVA solution [C]//Optoelectronic Devices and Integration. Optical Society of America, 2015: OW2C. 4.

[111] Guo B, Yao Y. Tunable triple-wavelength mode-locked fiber laser with topological insulator Bi_2Se_3 solution [J]. Optical Engineering, 2016, 55(8): 081315.

[112] Guo B, Yao Y, Yan P G, et al. Dual-wavelength soliton mode-locked fiber laser with a WS2-based fiber taper [J]. IEEE Photonics Technology Letters, 2016, 28(3): 323-326.

[113] Guo B, Li S, Fan Y, et al. Versatile soliton emission from a WS2 mode-locked fiber laser [J]. Optics Communications, 2018, 406: 66-71.

[114] Zhao R, Li J, Zhang B, et al. Triwavelength synchronously mode-locked fiber laser based on few-layered black phosphorus[J]. Applied Physics Express, 2016, 9(9): 092701.

[115] Yun L. Black phosphorus saturable absorber for dual-wavelength polarization-locked vector soliton generation [J]. Optics Express, 2017, 25(26): 32380-32385.

[116] Liu M, Zhao N, Liu H, et al. Dual-wavelength harmonically mode-locked fiber laser with topological insulator saturable absorber [J]. IEEE Photonics Technology Letters, 2014, 26 (10): 983-986.

[117] Luo Z, Huang Y, Wang J, et al. Multiwavelength dissipative-soliton generation in Yb-fiber laser using graphene-deposited fiber-taper [J]. IEEE Photonics Technology Letters, 2012, 24(17): 1539-1542.

[118] Huang S, Wang Y, Yan P, et al. Tunable and switchable multi-wavelength dissipative soliton generation in a graphene oxide mode-locked Yb-doped fiber laser[J]. Optics Express, 2014, 22(10): 11417-11426.

[119] Guo B, Yao Y, Yang Y F, et al. Dual-wavelength rectangular pulse erbium-doped fiber laser based on topological insulator saturable absorber [J]. Photonics Research, 2015, 3(3): 94-99.

[120] Zhao N, Liu M, Liu H, et al. Dual-wavelength rectangular pulse Yb-doped fiber laser using a microfiber-based graphene saturable absorber[J]. Optics Express, 2014, 22(9): 10906-10913.

[121] Gao L, Zhu T, Huang W, et al. Vector rectangular-shape laser based on reduced graphene oxide interacting with a long fiber taper [J]. Applied Optics, 2014, 53 (28): 6452-6456.

[122] Song Q, Wang G, Zhang B, et al. Passively Q-switched mode-locked dual-wavelength Nd: GYSGG laser using graphene oxide saturable absorber [J]. Optics Communications, 2015, 347: 64-67.

[123] Vengsarkar A M, Lemaire P J, Judkins J B, et al. Long-period fiber gratings as band-rejection filters [C]//Optical Fiber Communication Conference. Optical Society of America, 1995: PD4.

[124] Intrachat K, Kutz J N. Theory and simulation of passive modelocking dynamics using a long-period fiber grating [J]. IEEE Journal of Quantum Electronics, 2003, 39 (12): 1572-1578.

[125] Karar A S, Smy T, Steele A L. Nonlinear dynamics of a passively mode-locked fiber laser containing a long-period fiber grating [J]. IEEE Journal of Quantum Electronics, 2008, 44(3): 254-261.

[126] Guo B, Yang W L. Ultra-long-period grating as a novel tool for multi-wavelength ultrafast photonics [C]//AOPC 2017: Laser Components, Systems, and Applications. International Society for Optics and Photonics, 2017, 10457: 104572R.

[127] Manakov S V. On the theory of two-dimensional stationary self-focusing of electromagnetic waves [J]. Soviet Physics-JETP, 1974, 38(2): 248-253.

[128] Guo B, Yao Y, Tian J J, et al. Observation of bright-dark soliton pair in a fiber laser with topological insulator [J]. IEEE Photonics Technology Letters, 2015, 27(7): 701-704.

[129] Guo B, Yao Y, Xiao J J, et al. Topological insulator-assisted dual-wavelength fiber laser delivering versatile pulse patterns [J]. IEEE Journal of Selected Topics in Quantum Electronics, 2016, 22(2): 8-15.

[130] Li K X, Song Y R, Tian J R, et al. Analysis of bound-soliton states in a dual-wavelength mode-locked fiber laser based on Bi_2Se_3[J]. IEEE Photonics Journal, 2017, 9(3): 1-9.

[131] Zhao R, Li G, Zhang B, et al. Multi-wavelength bright-dark pulse pair fiber laser based on rhenium disulfide [J]. Optics Express, 2018, 26(5): 5819-5826.